

RANGING STUDIES WITH AN ULTRA-WIDEBAND,
PULSED, OPTOELECTRONIC THz BEAM SYSTEM

By

BRADLEY W. NICHOLSON

Bachelor of Science

University of Missouri-Rolla

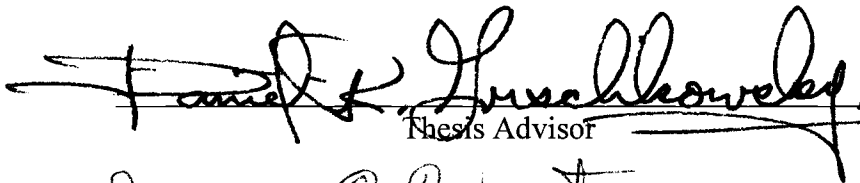
Rolla, Missouri

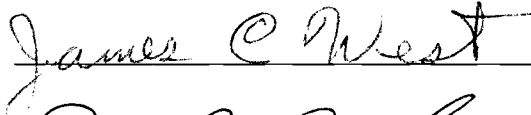
1992

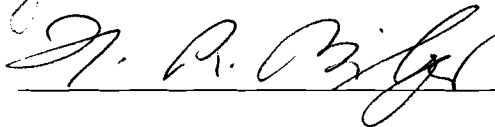
Submitted to the Faculty of the
Graduate College of the
Oklahoma State University
in partial fulfillment of
the requirements for
the Degree of
MASTER OF SCIENCE
May, 1995

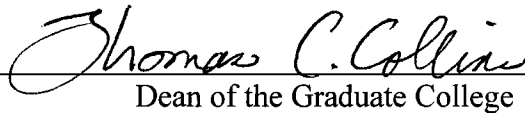
RANGING STUDIES WITH AN ULTRA-WIDEBAND,
PULSED, OPTOELECTRONIC THz BEAM SYSTEM

Thesis Approved:

 April 7, 1995
Thesis Advisor






Dean of the Graduate College

ACKNOWLEDGMENTS

I would like to thank my adviser Dr. Daniel Grischkowsky for his guidance throughout this research and for bringing this type of research opportunity to Oklahoma State University. I would also like to thank Dr. Alan Cheville for his ability to explain complicated processes in very simple terms and for his incredible patience.

I would especially like to thank my wife Kendra for being the most incredible human being on this planet. Special thanks to the unborn addition to our family for providing inspiration throughout these last seven months.

Final thanks go to all of my family for providing encouragement and believing in my abilities throughout the years.

TABLE OF CONTENTS

PREFACE.....	1
--------------	---

Chapter One

THz TRANSMITTER AND RECEIVER	3
Chip function	3
<i>Creating THz Radiation</i>	3
<i>Optical Lens Mount and Adjustment</i>	4
<i>Detecting THz Radiation</i>	4
Chip Mount	5
THz Beam Collimation.....	6
<i>THz (Silicon) Lens Mount and Adjustment</i>	7
Laser sources used	7
Dielectric optics combined with Al coated optics	8
Data Gathering	8

Chapter Two

PHYSICAL SETUP OF SYSTEM.....	10
Transmitter and Receiver Location.....	10
Problems Using VBS for Beam Steering.....	11
Elevated Table for Transmitter and Receiver	11
Movement Transferred From Optical Table	12
Noise Transferred From Chopper Motor	13

Frequency Dependent Noise	13
Airtight Enclosure	13
Difficulty in Reaching Receiver	15
Difficulty in Adjusting Stepper Motor.....	16
Method of Directing THz Beam Outward	16
Target Holder	16
EXPERIMENTAL TECHNIQUES	17
Use of Photodiodes to Determine Delay Between Pump and Probe Pulses	17
Adjusting Length of Coaxial Cable to Shift Pump and Probe to Straddle Sync Pulse.....	18
Scale to Facilitate Moving Delay Line When Performing Gross Timing Adjustments	18
Optical Alignment of THz Beam.....	19
Adjusting the Focus and Position of the Laser Spot.....	20
Justification for Using Si Lens on Receiver Chip.....	21

Chapter Three

DIAGNOSTIC EQUIPMENT	23
Autocorrelator	23
Spectrometer	25

Chapter Four

EXPERIMENTAL RESULTS.....	27
Signal Obtained While Tuning System.....	27
First Signals Obtained With Targets.....	29
First Signals Obtained From Targets at ~1 Meter.....	33

Retuning System and Detecting Smaller Targets	35
The Effect of Humidity	38
Maximum Detected Backscattered Signals From Vertically Oriented Targets.....	40
Summary of Results With Vertically Oriented Cylindrical Targets	44
The Effect of Target Orientation.....	46
Collimation Study	47
Results Obtained With a Spherical Target.....	50

Chapter Five

CONCLUSIONS AND FUTURE RESEARCH	54
BIBLIOGRAPHY.....	56

LIST OF FIGURES

Chapter One

Figure 1-1)	Gallium Arsenide THz Transmitter Chip	3
Figure 1-2)	Silicon on Sapphire THz Receiver Chip	5
Figure 1-3)	THz Beam Collimation	6

Chapter Two

Figure 2-1)	THz System Setup.....	10
Figure 2-2)	Elevated Table	12
Table 2-1)	Water Vapor Lines.....	14
Figure 2-3)	Airtight Enclosure.....	15

Chapter Three

Figure 3-1)	Functional diagram of autocorrelation unit used in this investigation.....	24
Figure 3-2)	a) Non-overlapping pump and probe pulse, b) Slightly overlapping pump and probe pulse, c) Totally overlapping pump and probe pulse.	25
Figure 3-3)	Functional diagram of spectrometer used in this investigation	26

Chapter Four

Figure 4-1)	First THz signal received with no reflection into enclosure.	27
--------------------	---	----

Figure 4-2)	Numerical Fourier transform of Figure 4-1.	28
Figure 4-3)	First backscattered THz signal received with 5.1 cm diameter mirror target located at 12 cm.	29
Figure 4-4)	Frequency domain representation of Figure 4-3.	30
Figure 4-5)	First backscattered THz signal received with a simple geometric object target (vertical cylindrical rod) located at 12 cm.	31
Figure 4-6)	Numerical Fourier transform of Figure 4-5.	31
Figure 4-7)	Determining contribution of unintended objects to overall signal received. The data obtained without a target has been offset by -15 pA for convenience.	32
Figure 4-8)	First backscattered THz signal received from a 5.1 cm diameter mirror at 98 cm.	33
Figure 4-9)	Numerical Fourier transform of Figure 4-8.	34
Figure 4-10)	Backscattered THz signal received from a vertical brass rod at 98 cm.	34
Figure 4-11)	Numerical Fourier transform of Figure 4-10.	35
Figure 4-12)	Best signal received with no redirection of THz beam into the enclosure.	36
Figure 4-13)	Numerical Fourier transform of Figure 4-12.	37
Figure 4-14)	"Cleaner" signal obtained after peaking system, redesigning target mount, and changing target mirror to a 10.2 cm square mirror.	37
Figure 4-15)	Numerical Fourier transform of Figure 4-14.	38
Figure 4-16)	The elliptical area illustrates the "smoother" late time response associated with lower humidity in the enclosure.	39
Figure 4-17)	Best signal received with vertically oriented 13.7 mm diameter brass rod at 1 meter.	40
Figure 4-18)	Numerical Fourier transform of Figure 4-17.	41
Figure 4-19)	Best signal received with vertically oriented 6.4 mm diameter copper tubing at 1 meter.	41
Figure 4-20)	Numerical Fourier transform of Figure 4-19.	42

Figure 4-21)	Best signal received with vertically oriented 3.2 mm diameter copper tubing at 1 meter.	42
Figure 4-22)	Numerical Fourier transform of Figure 4-21.	43
Figure 4-23)	Best signal received with vertically oriented 1.0 mm diameter copper wire at 1 meter.....	43
Figure 4-24)	Numerical Fourier transform of Figure 4-23.	44
Figure 4-25)	Comparison of detected signal strength for vertically oriented cylindrical targets of varying diameters located at 1 meter.	45
Figure 4-26)	Dependence of peak detected current on vertically oriented cylindrical target's diameter.	45
Figure 4-27)	Determination of the effect of target orientation on returned signal using horizontally oriented 13.7 mm diameter brass rod at 1 meter.	46
Figure 4-28)	Shifting target to determine frequency distribution within THz beam	48
Figure 4-29)	Comparison of spectrum for target centered in THz beam and shifted 17 mm perpendicular to beam path.....	48
Table 4-1)	Determining THz beam collimation	49
Figure 4-30)	Signal detected using 2.5 cm diameter brass sphere at 1 meter.....	51
Figure 4-31)	Numerical average of 4 data scans taken with 2.5 cm diameter brass sphere at 1 meter.....	51
Figure 4-32)	Comparison of signal detected with and without averaging using 2.5 cm diameter brass sphere at 1 meter.	52
Figure 4-33)	Numerical Fourier transform of Figure 4-31.	53

PREFACE

The purpose of this investigation was to determine the feasibility of utilizing an ultra-wideband optoelectronic THz beam system for ranging measurements. The system¹ was developed at the IBM Watson Research Center by Dr. Daniel Grischkowsky's research group. Although it has never been used for ranging measurements, the system has previously been used for THz time-domain spectroscopy.^{2,3}

In evaluating the capabilities of this THz beam system, signals were obtained by scattering a well-collimated pulsed beam of freely propagating radiation from simple geometric conducting objects. The bulk of the experimentation was done with cylindrical objects with diameters as small as 1.0 mm at distances of up to 1 meter. Results were also obtained for a 2.5 cm diameter sphere at 1 meter. The transmitted signal had frequency components ranging from 100 GHz to over .5 THz.

The use of ultra-wideband systems to perform scattering measurements has previously been studied with varying targets and much lower frequency ranges.⁴⁻⁶ Carin and Agi have reported on a laser-based system that produced "freely propagating bursts of picosecond duration electromagnetic radiation, with a bandwidth extending from 5 to over 70 GHz."⁴ In their paper, targets consisting of one conducting strip, two conducting strips, and a conducting sphere were used. They present their gathered data as well as an evaluation of the fit of this data to theoretical expectations. For their case, the distance of the conducting sphere from the transmitter was 7.0 cm while the distance from the receiver was 5.5 cm. The 7.0 cm distance corresponds to ~16 wavelengths in separation between the target and transmitter. For comparison, the results for the conducting sphere reported in this experiment were obtained at a distance of 1 meter. This corresponds to the target being located over 1700 wavelengths from the transmitter and receiver.

The goal of the research described here is to simply demonstrate the ability to use the system developed by Grischkowsky for ranging measurements; therefore, a detailed evaluation of the fit of gathered data to theory will not be presented.

CHAPTER 1

THz TRANSMITTER AND RECEIVER

Chip function

The structure and operation of the chips used as transmitter and receiver in this investigation are explained in detail in N. Katzenellenbogen and D. Grischkowsky's report on an ultra-wideband optoelectronic THz beam system.⁷ Following is a general description of construction and function of the chips used in this system.

Creating THz Radiation

The chip used as a transmitter in this experiment utilizes a Gallium Arsenide (GaAs) substrate with coplanar metal lines on the surface configured as shown in Figure 1-1 below.

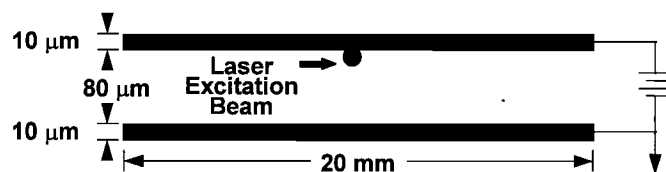


Figure 1-1) Gallium Arsenide THz Transmitter Chip

As indicated, the metal lines have a width of $10\ \mu\text{m}$ with an $80\ \mu\text{m}$ separation between the lines. The total length of the lines is $20\ \text{mm}$. The $1\ \mu\text{m}$ thick lines are fabricated of a Ni, Au, and Ge alloy. This transmitter will be referred to hereafter as a

10-80-10 TX. In this investigation the transmitter, as well as the receiver, is mounted such that the coplanar strips are oriented vertically.

This type of transmitter chip generates bursts of THz radiation. This is accomplished by focusing the beam of a Ti-Sapphire laser onto the photoconductive gap between the parallel 10 μm transmission lines on the GaAs chip. The beam must be focused on the inner edge of the positively biased transmission line. The Ti-Sapphire laser produces 825 nm, ~ 100 fsec pulses at an 82 MHz repetition rate. Laser beam power incident on the receiver and transmitter is on the order of 20 mW.

A burst of THz radiation is generated each time a laser pulse is incident upon the chip. When the laser pulse arrives at the surface of the chip, free carriers are created. The region in which these free carriers are created has a very high electric field which accelerates the carriers, thus inducing current in the substrate.

With this configuration, the bursts of THz radiation that are created are horizontally polarized.

Optical Lens Mount and Adjustment

The optical lenses used to focus the laser beam onto the chip have a focal length of 6 mm and were secured to small aluminum brackets with epoxy glue. These brackets were secured to a Newport 642 XYZ translation stage. This enabled precise positioning of the lens. This allows adjustments to the position of the laser spot once it has been focused on the chip. In creating or detecting THz radiation with this setup, it is necessary to have very precise control of the laser spot positioning. In this interest, differential micrometers were used in the X and Z portions of the XYZ translation stage.

Detecting THz Radiation

The receiver chip utilizes a Silicon-on-Sapphire (SOS) substrate and has a somewhat different antenna structure than that of the transmitter chip. Similar to the

transmitter chip, the receiver chip has coplanar metal lines on the surface which are $10\ \mu\text{m}$ wide; however, the separation between lines is $120\ \mu\text{m}$. On this chip, a Hertzian dipole antenna is imbedded in the coplanar transmission line. The photoconductive gap between the arms of the dipole antenna is $5\ \mu\text{m}$ wide. The physical setup of this receiver chip is shown below in Figure 1-2. The ammeter shown in the diagram actually represents an Ithaco 1211 Current Preamplifier and Stanford Research Systems SR350 Lock-In amplifier used in combination.

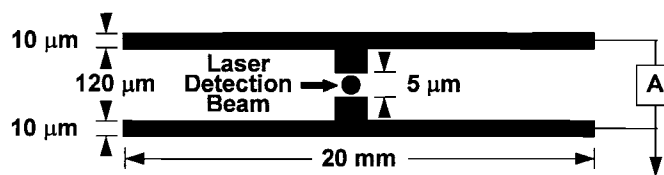


Figure 1-2) Silicon on Sapphire THz Receiver Chip

When the incoming THz beam is focused on the $5\ \mu\text{m}$ gap, the horizontally polarized E-field induces a voltage potential between the vertically oriented lines on the receiver. Therefore, if the photoconductive gap is illuminated at the time the THz signal is present, the free carriers created within the area which has a potential difference will result in a small current being induced. In this investigation, induced current is usually in the nanoampere or picoampere range and can be easily detected with a current amplifier. The amount of current detected directly relates to the strength of the incident THz signal.

Chip Mount

Both the transmitting and receiving chips were mounted in plastic holders fabricated at the IBM Watson Research Center. The holders were placed in precision X-Z translation stages to aid in alignment of the apparatus. The Z translation stage

consisted of a micro-adjustable screw-type mount while the X translation stage was a Newport 640 Series.

THz Beam Collimation

When the THz radiation is created and begins to propagate, it is collimated by a silicon lens designed specifically for this system. The propagating THz radiation is then further collimated by an electroformed nickel off-axis paraboloidal mirror coated with rhodium. The resulting highly collimated beam has the highest frequencies located in the center of the beam, with frequency sweeping to the lowest frequency components on the extreme edge of the beam. The transmitter chip, Si lens, and paraboloidal mirror combination are shown in Figure 1-3.

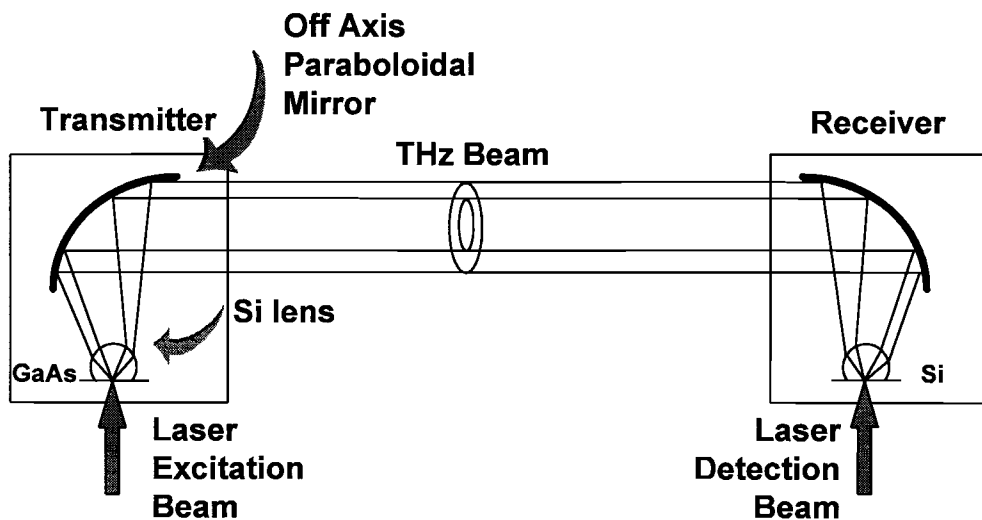


Figure 1-3) THz Beam Collimation

This operation is reversed for the receiver stage of this system as illustrated in Figure 1-3.

THz (Silicon) Lens Mount and Adjustment

A silicon lens identical to the one used to collimate the outgoing THz beam at the transmitter enabled recollimation of the THz beam incident upon the receiver. Semi-hemispherical in shape and 5 mm thick, these special order lenses are composed of high-resistivity single crystal silicon.

The lenses mount directly against the back surface of the SOS or GaAs chip, as shown in Figure 1-3, to reduce reflection from the interface back into the chip itself. They are held in place by pressure from a spring and collar within a modified Newport Fiber Optic Coupler. The modifications were done by Dr. Nir Katzenellenbogen. The modified coupler allows for adjustments of lens position in the X and Z directions as necessary. This provides a way to adjust the lens so that the point of generation of THz radiation on the transmitter coincides with the focal point of the lens to allow for maximum transmission of the signal generated. In the same manner, the lens on the receiver may be positioned such that the focal point of the lens lies at the same point as the gap on the receiving antenna.

In the THz frequency range, the silicon used in the lenses has an index of refraction of approximately 3.42.³ Thus, a propagation distance of 5 mm within the lens corresponds to 1.7 cm of propagation in free space. This consideration becomes important when trying to find THz signals without either one or both lenses.

Laser sources used

In creating THz radiation with the method used in this investigation it is necessary to use an extremely fast laser source. The laser used in the experiment was a commercial Spectra Physics Tsunami Ti-Sapphire laser, which utilized a folded cavity and was configured to produce pulse widths on the order of 100 femtoseconds. A Spectra Physics Beamlock Argon ion laser source was used to drive the Ti-Sapphire laser. The Tsunami

has a tuning range of 780-900 nm and an 82 MHz repetition rate. For this investigation the laser was operated around 840 nm with an approximate output power of 500 mW. All of these parameters varied slightly daily, making it necessary to take reference scans at the start of every experimental run.

Operating at 82 MHz corresponds to a physical separation between pulses of 12.2 nsec, or ~ 3.66 meters. This relates directly to an ~ 3.66 meter separation between the generated THz pulses.

Dielectric optics combined with Al coated optics

In beam steering, a combination of dielectric and aluminum coated mirrors were used. The dielectric mirrors used were optimized for near infrared radiation such as that contained in the Ti-Sapphire beam. The Al coated mirrors were not optimized and exhibit greater loss on reflection than do the dielectric mirrors. Therefore, as many dielectric mirrors as possible were used to deliver the maximum possible strength pulse train to the transmitting and receiving chips. This resulted in 500 mW of beam power being delivered to the THz setup. Of this, only 20-30 mW was required for proper system operation. A variable beam splitter was used to limit the delivered beam power to the desired level.

Data Gathering

The THz pulses created are optoelectronically sampled in a synchronous manner.⁷ Once the beam of THz pulses is created, it is mechanically chopped before striking the first paraboloidal mirror. Chopping frequency was on the order of hundreds of Hz. Care was taken to avoid chopping near any multiple of 60 Hz to avoid the high amount of ambient noise present at these frequencies. There was a problem with noise which varied with chopping frequency. This problem is discussed later in Chapter 2. The chopping frequency was used as the reference frequency for the lock-in amplifier mentioned earlier.

Recording of data was accomplished with a personal computer utilizing an analog to digital (A/D) converter and the Viewdac 2.2 data acquisition software package. The custom programming necessary for this experiment was accomplished in a collaborative effort between Dr. Alan Cheville and Tae-In Jeong.

CHAPTER 2

PHYSICAL SETUP OF SYSTEM

Transmitter and Receiver Location

The transmitter and receiver sections were located adjacent to one another in an arrangement similar to those used in previous experiments with this type of source and receiver.^{1-3,7} The chips are positioned adjacent to one another and oriented such that they are both pointing in the same direction, as shown in Figure 2-1. As with the previous setups, paraboloidal mirrors are used to achieve a well-collimated THz beam from the transmitter and to direct this beam onto the receiver.

The setup used in this experiment differs from that of earlier experiments in that a set of mirrors (the redirecting mirrors) was constructed to slide on a rail into the collimated beam to direct the THz radiation into the airtight, ranging enclosure described in detail later in this chapter. This is shown in Figure 2-1. After the system is tuned, the redirecting mirrors can be moved into the THz beam to direct the beam toward a target.

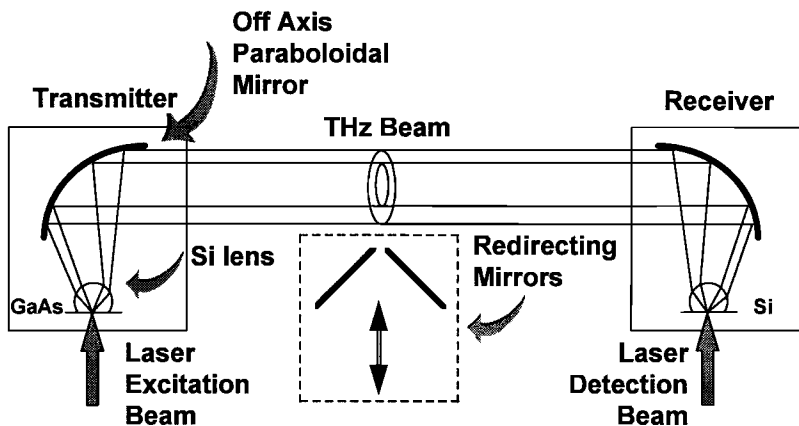


Figure 2-1) THz System Setup

Problems Using VBS for Beam Steering

Initially, the variable beam splitter (VBS) served a dual purpose. In addition to attenuating the incoming optical beam to the desired level, the beam splitter was used for beam steering. The beam had to be attenuated from the incoming 500 mW of beam power to approximately 40 mW. This 40 mW beam was then passed through a 50/50 beam splitter to power transmitter and receiver. To attain this 460 mW attenuation it was necessary to set the VBS such that the incoming beam was incident upon a section which had a small amount of "silvering." Unfortunately, this allowed for reflections from the second surface of the VBS. This reflection resulted in the outgoing beam having a double-lobe pattern which was difficult to work with and gave unsatisfactory results.

This problem was rectified by positioning the VBS to serve strictly as an attenuator. A dielectric mirror was used to steer the beam as necessary.

Elevated Table for Transmitter and Receiver

A concern when designing this experiment was the possibility of receiving a signal that was not reflected from the intended target. One way for this to happen is for the THz beam to strike something other than the intended target. A well-collimated beam will help ensure that this does not happen. The collimation of the obtained THz beam was studied and is presented in detail in chapter 4.

Another possible problem is receiving a signal reflected from an object after the beam has struck the intended target. This phenomenon leads to dual paths of differing lengths. To help eliminate the effect of possible specular reflection from the surface of the optical table the transmitter and receiver were placed on an elevated breadboard. The legs supporting the breadboard were fabricated from 3.8 cm diameter aluminum rod and were designed to be adjustable between 15 cm and 28 cm. The table was placed at 25 cm for this experiment.

Elevating the apparatus in this manner accomplishes two things. First, the elevation of the table means that any specular reflection from the optical table must traverse 12 cm more than any signal reflected directly from the target. This is shown below in Figure 2-2.

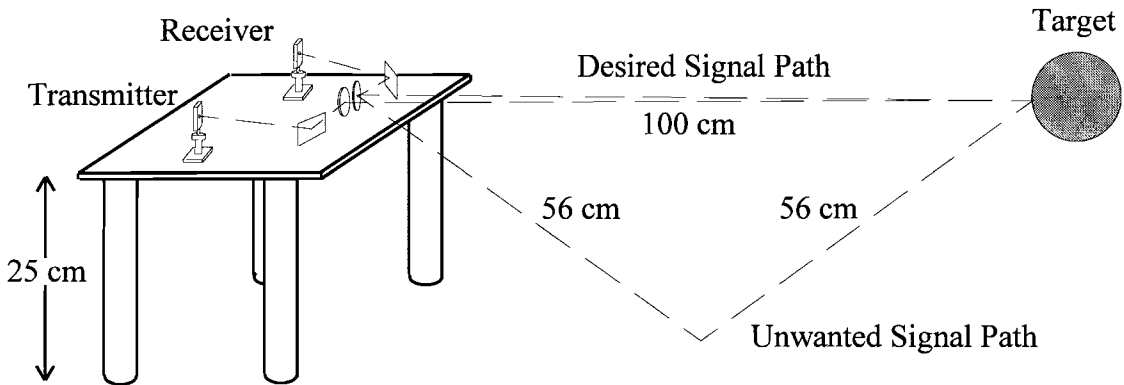


Figure 2-2) Elevated Table

The longest scan taken during this investigation was 70 psec which corresponds to a distance of only $70 \cdot 10^{-12} \text{ s} \times 2.998 \cdot 10^{10} \frac{\text{cm}}{\text{s}} = 2.1 \text{ cm}$. This puts the specular pulse well behind the pulse intended for reception. Given the 82 MHz repetition rate of the Ti-Sapphire laser, the physical separation between THz pulses is ~ 3.66 meters. The second way elevating the table diminishes the chance of receiving specular reflections is the angle of incidence of the specular pulse upon the redirecting mirror. The angle of incidence is sharp enough that the specularly reflected pulse would not be focused onto the receiving antenna.

Movement Transferred From Optical Table

During data gathering, it was noted that the received signal was affected by movements of the optical table. This problem was avoided by not working on the optical

table while data was being gathered. Some mechanical instability in the system is the most probable cause of this sensitivity.

Noise Transferred From Chopper Motor

As system noise was being tracked down, it was noted that the elevated table to which the transmitter and receiver were attached vibrated when the chopper motor was operating. This problem was alleviated by mounting the chopper motor directly to the optical table instead of the elevated platform. The chopper motor was mounted on a tall brass rod to elevate it back to its original height.

Frequency Dependent Noise

During the course of data gathering, it was noticed that the amount of noise the current amplifier received with no signal present varied with the chopping frequency. A high degree of noise is expected around harmonics of 60 Hz; however, there was a good deal of noise located at other frequencies.

In attempting to identify some causes of the high amount of system noise, the output of the current amplifier was fed to a digitizing oscilloscope for examination of its spectral content. In addition to the expected noise at multiples of 60 Hz, it was seen that significant noise was present at frequencies other than these. The exact location of noise spikes varied daily. Turning off the room lights eliminated some of the observed noise.

Airtight Enclosure

With freely propagating radiation in the THz range, interaction with ambient water vapor becomes a significant factor in signal quality. Dispersion and absorption associated with water-vapor lines have a marked effect on the late time response of any returned signal. Martin van Exter, Ch. Fattering, and D. Grischkowsky used THz equipment similar to that used in this experiment to accurately determine the location of

various water-vapor lines and their associated absorption coefficients.² As explained in the paper, the values listed are peak-intensity coefficients for a 1 meter path at 100% humidity in 1 atm of nitrogen. The results are shown in the following table:

Table 2-1) Water Vapor Lines²

Water-Vapor Line Location (THz)	Absorption Coefficient
.557	9.4
.752	6.9
.988	5.0
1.097	32.0
1.113	10.1
1.163	37.9
1.208	9.8
1.229	8.5
1.410	23.1

To provide a means of limiting the effects of water vapor, the entire apparatus was placed within an airtight enclosure. This allowed for reducing the humidity for the entire path of the THz beam by purging the enclosure with air having a low water vapor content. Two such air sources were available: a high volume flow of air used for optical table flotation (~20% relative humidity) and a lower volume flow of air filtered through a Balston 75-62 FT-IR Purge Gas Generator. The humidity of the air produced by the purge gas generator is below the minimum measurable value of the hygrometer. Relative humidity was measured using a Fisher Scientific Model 11-661-7B digital hygrometer. The working range of this hygrometer is 5% to 95% relative humidity.

One air tube of the high volume flow and two air tubes of the lower volume flow were installed in the enclosure. This allowed for a fast purge down to the humidity level of the optical table air followed with slower purging using the filtered air until the ~5% relative humidity was attained.

The airtight enclosure was 81 cm tall with a 66 cm by 244 cm footprint with a frame constructed of 2.5 cm aluminum angle bracket and oak 2.5 cm by 2.5 cm supports. Doors were made of Plexiglas while other surfaces were covered with 20 mil vinyl sheeting. Seals were made with common duct tape. A schematic representation of the box is shown below in Figure 2-3.

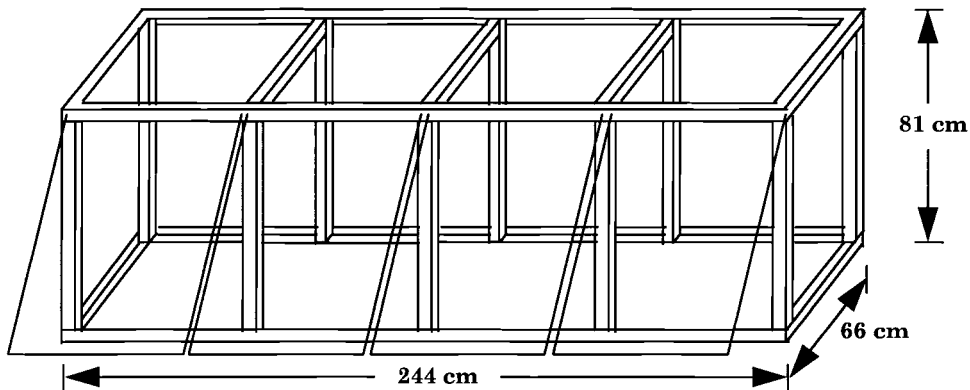


Figure 2-3) Airtight Enclosure

Difficulty in Reaching Receiver

With the airtight ranging enclosure construction as shown in Figure 2-3, the receiver unit was located at the back of the optical table as well as at the back of the enclosure. This made it very difficult to reach the receiver when making necessary adjustments. One very difficult task was positioning the optical beam when initially aligning the system. This was due to the difficulty in positioning the viewing microscope necessary for observing the position and focus of the optical beam, while the beam was being adjusted to strike the chip, such that the laser spot was incident upon the photoconductive gap of the receiver.

Difficulty in Adjusting Stepper Motor

It was necessary to remove and replace three back panels on the airtight enclosure to make any adjustments to the stepper motor. This inconvenience could have been avoided by enlarging the footprint of the enclosure to include the entire delay line; thereby, eliminating the need to remove any panels from the back of the enclosure.

Method of Directing THz Beam Outward

Having a "traditional" configuration for the THz setup, see Figure 2-1, allowed for simple tuning of the system. After a signal was attained and the system was tuned to achieve maximum signal strength, the THz beam had to be directed out into the enclosure in a controlled manner. This was accomplished by designing a set of mirrors which could be easily inserted into and removed from the beam. These can be seen in the lower center portion of Figure 2-1. This process had to be repeatable. To ensure this, a rail with a mm scale affixed was used as a base for a sliding mount. A set of 5.1 cm diameter Al coated mirrors was placed on the sliding mount. These mirrors were mounted in Newport MM1-A adjustable optical mounts to allow for adjustments to the tilt of the mirror to facilitate THz beam steering.

When the sliding mirrors were inserted into the beam of THz radiation, they were situated such that their centers were located on the centerline of the THz beam.

Target Holder

In the first measurements with a target, the target holder consisted of a brass rod inserted into a standard base. For the scans taken at 12 cm, the holder was placed on a 10 cm square aluminum plate attached to the elevated table. All scans taken at 98 cm were taken with this type of holder with a much longer brass rod. The target was simply attached to the top of the rod.

Vibrations being passed from the optical table into the target and holder resulted in the target's positioning being unstable. Given that $300\ \mu\text{m}$ of propagation correlates to $\sim 1\ \text{psec}$, vibrational movement on the μm scale will affect measurements substantially. The instability of the target's position led to poor returned signal quality.

Subsequently, the original mount was replaced with a much more stable configuration. The mount that replaced the original was constructed from $3.8\ \text{cm}$ diameter aluminum rod firmly attached to the optical table. On top of this rod, a X translation stage was attached. This was done to allow horizontal movement of the target perpendicular to the generated beam. A Z translation stage was attached to the X translation stage to allow for controllable vertical adjustment of the target within the beam. This mount proved to be effective and was used throughout the remainder of the experiment.

EXPERIMENTAL TECHNIQUES

Use of Photodiodes to Determine Delay Between Pump and Probe Pulses

In aligning the THz system, it is essential that the time delay between the incidence of the pump pulse on the transmitter and the incidence of the probe pulse on the receiver be known. For detection of THz radiation, the time delay between pump (creation of THz) and probe (detection of THz signal) should be equivalent to the time required for the generated THz pulse to propagate from transmitter to receiver .

There are several ways of determining this timing. One method is to physically measure the optical path length that the pump and probe pulse traverse and compare these. This can be done very roughly using string to measure accessible optical paths and using approximations of optical path length in inaccessible areas. This method proves very cumbersome if, as in this experiment, the optical paths are not easily accessible. When using this method, errors are introduced by incorrectly measuring the optical

path--i.e., assuming a beam strikes the center of a directing mirror when it actually strikes the mirror off-center--and incorrect assumptions on the path traversed inside an object such as a retroreflector.

Another possible method allows for determining the time delay between the pump and probe pulse electronically. This method employs fast photodiodes and was utilized in determining system timing in this experiment. By placing a fast photodiode in the mount for the chip, either transmitter or receiver, it is possible to obtain a signal that directly correlates to the incident laser pulse train. The obtained signal may be displayed on an oscilloscope versus the monitor pulse train available from the laser head control unit. The monitor pulse train should be used as the trigger.

This process is done after the translational mounts have been adjusted to focus the Ti-Sapphire beam onto the proper point.

Adjusting Length of Coaxial Cable to Shift Pump and Probe to Straddle Sync Pulse

When measuring the time delay between the monitor (trigger) pulse and the detected pulse it is desirable to use the highest temporal resolution possible. To do this, the detected pulses are manipulated such that they straddle the trigger pulse. This allows for maximum accuracy.

The simplest way to adjust the position of the detected pulses in relation to the trigger pulse is to insert a delay in the line until the pulses are properly positioned. In this investigation, this was accomplished by adding short lengths of coaxial cable to the sampling lead of the signal analyzer.

Scale to Facilitate Moving Delay Line When Performing Gross Timing Adjustments

When working with a target range out to 1 meter, it becomes necessary to have a variable delay line that allows for adjustment over the entire range. As the maximum adjustable range of the stepper motor is on the order of 20 cm, it was necessary to move

the entire stepper motor unit within the delay line. This movement had to be done frequently; therefore, repeatability was key to speeding system adjustments. Of great importance was that the stepper motor move on a line collinear with the optical path. This ensures that the Ti-Sapphire beam does not "walk around" on the optics and cause the detection beam to move on the receiving chip.

To accomplish this, a 244 cm section of 2.5 cm by 2.5 cm aluminum angle was clamped to the optical table. This served as a guide for the stepper motor unit to slide against when adjustments were made to its position.

A Helium Neon laser which was set up to be collinear with the Ti-Sapphire beam was used for alignment of this guide. The optical path was intercepted and the beam was redirected down the entire length of the optical table such that it was incident on an aperture. Adjustments were made to the position of the Aluminum guide until no change in the position of the laser spot on the aperture was observed as the stepper motor was moved to the extremes of the guide.

After final adjustments had been made to the guide position, apertures were positioned at opposite ends of the guide to facilitate realignment of the optical beam in the event of system disturbance. The fact that the retroreflector was mounted on a kinematic, or removable, base allowed the apertures to be positioned such that they were centered on the optical beam without disturbing the position of the stepper motor unit.

Optical Alignment of THz Beam

In aligning the THz portion of the system, accurately determining the position of the THz beam was essential. To accomplish this, a THz signal was obtained with no reflection into the enclosure. With this signal tuned up, apertures were inserted into the beam to determine the beam's center. After accurately determining the center of the beam, a HeNe laser was set up so that its propagation path was coincident with the center of the THz beam.

The mirror used to direct the HeNe beam along the THz path was mounted on a kinematic base to allow the mirror to be repeatably removed and replaced without affecting its position. This allowed for fairly quick and simple alignment of the redirecting mirrors and positioning of the intended target within the beam without disturbing the system. When aligning the system, the redirecting mirrors and the targets were positioned such that the HeNe, being collinear with the THz beam, was incident upon the approximate center of the optics used.

To simplify determining the point of incidence of the HeNe on the receiver chip, a small piece of lens cleaning tissue was placed on the back of the receiver during adjustments. This was done to reduce the glare due to reflection of the HeNe off the Silicon collimating lens present on the back of the receiver chip.

When the cylindrical targets were used, aluminum foil was wrapped around the target with the shiny side facing outward to enhance the target's reflection of the HeNe beam. The spreading of the HeNe beam could be seen in the enclosure when the room lights were turned off. This allowed for positioning of the target such that the reflection associated with the center of the beam was incident, to the greatest extent possible, upon the receiver's collimating lens. After proper positioning was attained, the foil was removed.

Adjusting the Focus and Position of the Laser Spot

Rough adjustments are made to the focus and position of the laser spot on the chip by aligning the chip and optical lens while observing the placement of the spot through a microscope. Due to the translucent nature of the chip, this proves to be a very difficult adjustment. This is further complicated by the necessity of having to position the microscope such that it is fairly oblique to the chip making the view difficult to interpret.

Fine adjustments are made via electronic means. Dr. Alan Cheville discovered a method of adjusting the focus and position of the laser spot without applying a bias

voltage to the antenna of interest. In previous investigations with this type of transmitter and receiver, the incoming laser beam was chopped at a low frequency and applied to the chip being adjusted. A received signal could then be simulated by applying a slight bias voltage to the receiver's or transmitter's antenna. As in normal detection, the incidence of the laser pulse creates free carriers which are accelerated in the potential. These free carriers create the small current being measured by the current amplifier.

It was found that the bias voltage was not necessary for some chips. The detected current exhibits maximum strength when the laser spot is properly aligned with the components on the chip. This technique allowed alignment of the system without having to apply an artificial bias to the extremely sensitive antenna on the receiving chip.

Although this effect is thought to result from the bias induced by stray EM signals in the laboratory, the effect is not fully understood.

Justification for Using Si Lens on Receiver Chip

In "Ultra-Wideband Transient Microwave Scattering Measurements Using Optoelectronically Switched Antennas" by Lawrence Carin and Kamil Agi⁴, they have the point of view that using a lens on the receiver is a poor choice due to its camouflaging of "physical effects associated with EM radiation." This camouflaging arises due to the returned signal having a distribution across the mentioned optics. The distance at which the targets are located in this THz experimentation virtually eliminates signal variation over the small angle which the detecting mirror subtends within the ~2 meter diameter spherical area which the outgoing pulse could be scattered.

Although the variation of the signal over the area of the detecting mirror is negligible, this was taken into consideration. However, the purpose of this experiment was to observe returned signals, not to compare them to theoretical values. Using a lens on both the transmitter and receiver yields vastly improved signal strength, thereby increasing the signal to noise ratio.

In later experimentation--and in contradiction with their earlier viewpoint--Carin, Rahman, and Kralj⁶ utilized fused silica hemispherical lenses in front of both the transmitting and receiving antennas to enhance the signal to noise ratio.

CHAPTER 3

DIAGNOSTIC EQUIPMENT

Autocorrelator

Given the femtosecond duration of the pulses in the Ti-Sapphire beam, it is necessary to use an autocorrelator in determining pulse width. A variable beam splitter is used to direct a portion of the optical beam into the autocorrelation chamber. Once inside the autocorrelation chamber, the beam is run through a 50/50 beam splitter to create two equal legs of the optical beam. For the autocorrelation to work, one leg must have an optical path length which varies with respect to the other. This is commonly referred to as the probe while the pulse train having a fixed optical path length is referred to as the pump pulse train. To attain a varying optical path length, one leg of the beam is directed into a retro-reflector attached to a simple audio speaker. This calculated horizontal translation relates directly to the change in total optical path length for the probe pulse train. A simple schematic of this type of autocorrelator is shown in Figure 3-1.

With no signal driving the speaker, the optical path lengths of the separate legs are set to be equal at the point that they are incident upon a nonlinear crystal. This should correspond to the point at which the two pulse trains coincide. Any divergence from this point will lead to a reduced overlap of the two pulses until there is eventually no overlap between the probe and pump pulses.

When a pulse from either the pump or the probe pulse train is incident upon the nonlinear crystal, second harmonic light is generated. Due to conservation of momentum, this second harmonic light follows the same path as the optical beam upon departure from the crystal. The two incident beams, probe and pump, are set so that they

are each incident upon the nonlinear crystal near the phase matching angle. Again, the path of the generated second harmonic light will be determined by applying conservation of momentum. The second harmonic light generated due to both optical beams can be easily isolated by placing a thin slot before the photodetector, effectively blocking any light generated along either beam path.

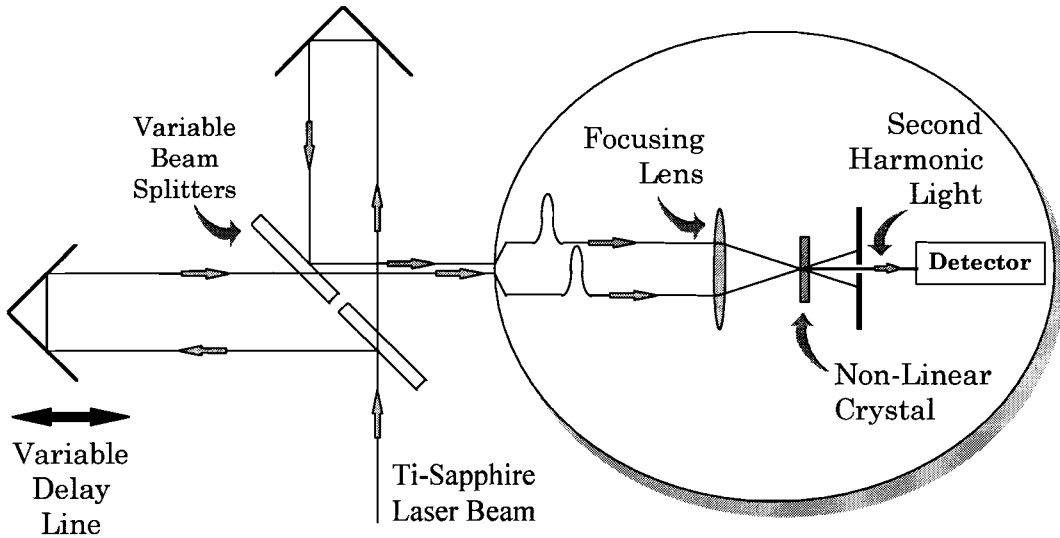


Figure 3-1) Functional diagram of autocorrelation unit used in this investigation

The voltage signal from the photodetector is fed to a Tektronix 2213A oscilloscope which displays the autocorrelation trace. This trace will be present only when the pump and probe pulses overlap. This is illustrated in figures 3-2a, 3-2b, and 3-2c below. As indicated, the amount of second harmonic light generated increases with the amount of overlap between the pump and probe pulses.

Due to the pump and probe pulses being identical, the autocorrelation trace is a known width in comparison to the original pulse width. Therefore, it is possible to calculate the width of the original pulse from the information contained in the autocorrelation trace. To accomplish this, an assumption must be made regarding the shape of the original pulses. After assuming a pulse shape for the original pulses in the

laser beam, their width can be accurately and easily calculated by applying standard autocorrelation techniques.⁸

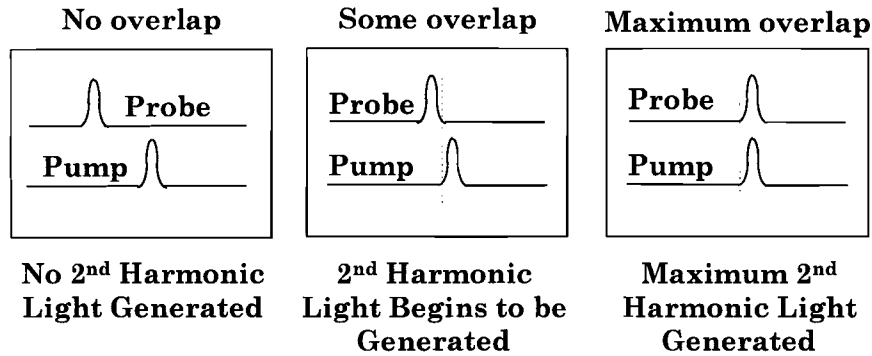


Figure 3-2 a) Non-overlapping pump and probe pulse,
 b) Slightly overlapping pump and probe pulse,
 c) Totally overlapping pump and probe pulse.

Spectrometer

To determine the frequency content of the pulses obtained from the Ti-Sapphire laser, it is necessary to utilize a spectrometer. This spectrometer uses a portion of the same beam that the autocorrelator described above does. The Ti-Sapphire beam is passed into the spectrometer where it strikes a diffraction grating. The diffraction grating spatially separates the various frequency components. The resulting diffraction pattern is directed onto a diode array. The physical separation of the diodes within the array makes it possible to determine the relative magnitudes of the different frequency components that constitute the Ti-Sapphire pulse. Current practice is to calibrate the spectrometer with a readily available HeNe laser source. This is done for convenience as the spectral lines of the HeNe laser are well known.

A diagram depicting the functionality of the spectrometer is shown in Figure 3-3. The actual spectrometer utilizes a combination of lenses to ensure correct imaging of the source onto the diffraction grating and similar imaging onto the diode array.

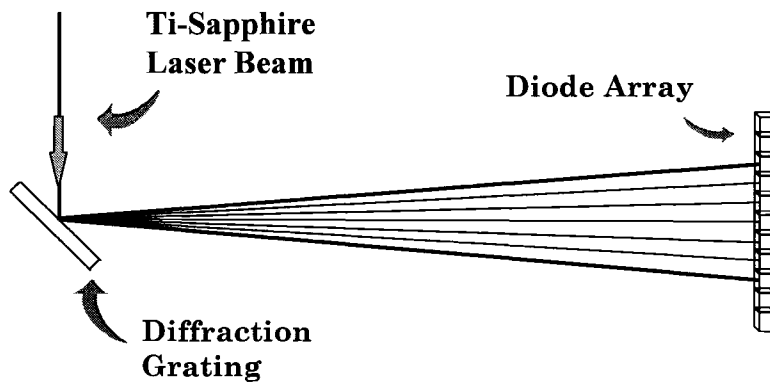


Figure 3-3) Functional diagram of spectrometer used in this investigation

Both the autocorrelator and spectrometer were used as diagnostic equipment in this investigation. Their primary function was to monitor the Ti-Sapphire laser's output beam. The trace obtained from the autocorrelator allowed for time domain observation of the laser pulse being produced, while the spectrometer allowed for frequency domain observation of the laser pulse being produced.

CHAPTER 4

EXPERIMENTAL RESULTS

In the course of this investigation, much time was spent setting up the system and trying to obtain the initial THz signal. After changing transmitter and receiver setup, discovering damaged chips, and discovering objects--such as spider webs--blocking the optical beam, a THz signal was finally obtained.

Signal Obtained While Tuning System

Figures 4-1 and 4-2 represent the time and frequency domain representations of this first signal obtained. This data was taken with no redirection of the THz beam out into the enclosure described in Chapter 2.

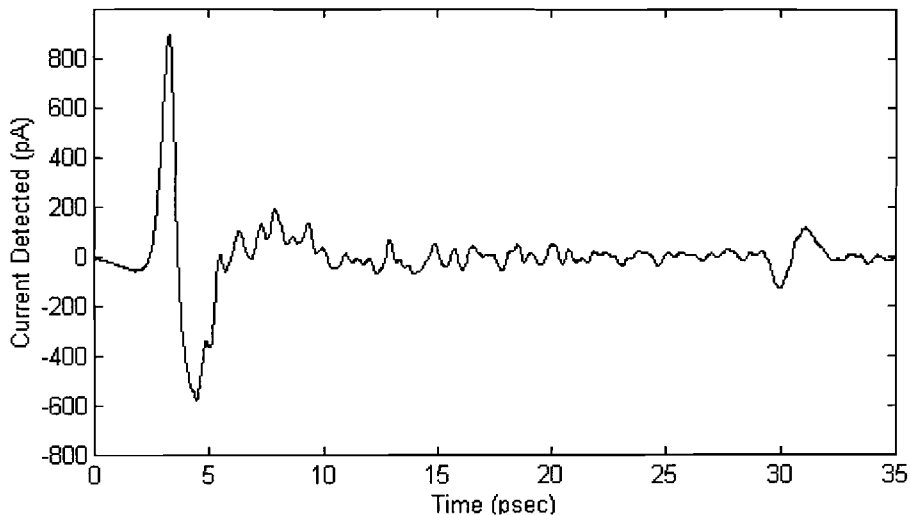


Figure 4-1) First THz signal received with no reflection into enclosure.

In Figure 4-1, a primary pulse can be seen that lasts approximately 4 psec and has a maximum amplitude that corresponds to a detected current of 900 pA. It can be seen in Figure 4-1 that the minimum-to-maximum separation for this pulse is 1.17 psec.

In the time domain representation, a secondary reflected pulse can be seen at 30 psec. The time separation between pulses is 26.7 psec. After the phase of research being reported in this paper was completed, Dr. Alan Cheville discovered that the secondary pulse was being introduced into the system by the laser steering optics. A variable beam splitter was responsible for creating a "ghost" pulse train. The secondary reflected pulse contributes to the rapid oscillatory nature of the received signal's relative magnitude in the frequency domain as shown in Figure 4-2.

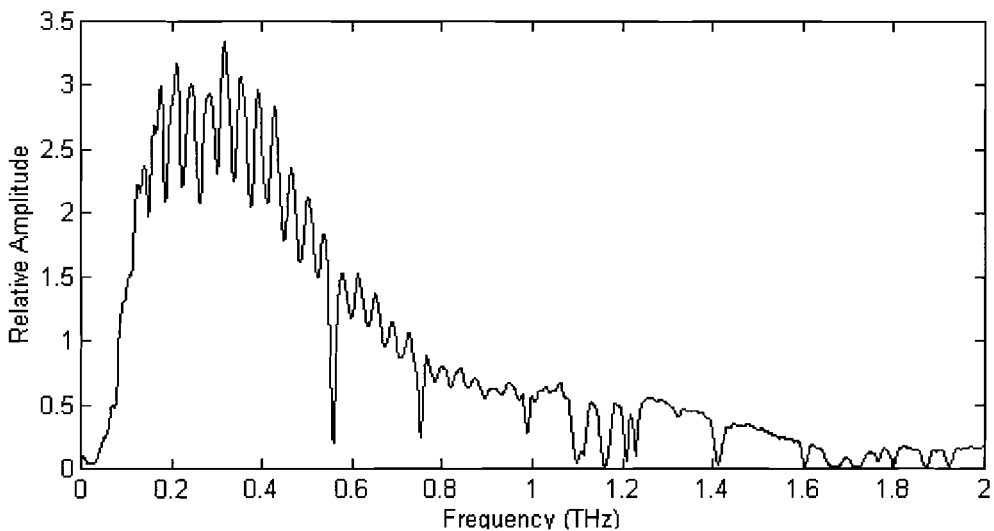


Figure 4-2) Numerical Fourier transform of Figure 4-1.

The numerical Fourier transform indicates that the detected signal has frequency components ranging from ~100 GHz to over 1 THz. The noticeable localized reductions in magnitude can be attributed to water vapor as will be explained in detail later in this chapter.

First Signals Obtained With Targets

As the above results were obtained with no reflection into the airtight enclosure, the next logical step was to try scattering the THz signal from a target in the enclosure. To do this, the redirecting mirrors were placed in the THz beam and a 5.1 cm diameter Al coated mirror was placed 12.0 cm from the first redirecting mirror and 11.5 cm from the second redirecting mirror. To align the redirecting and target mirrors such that the THz beam would be focused onto the receiver, a HeNe laser was used to optically align them as described in Chapter 2. The first successful scan is shown below in Figure 4-3. This is believed to be the first demonstrated ranging measurement with a bandwidth extending over .5 THz.

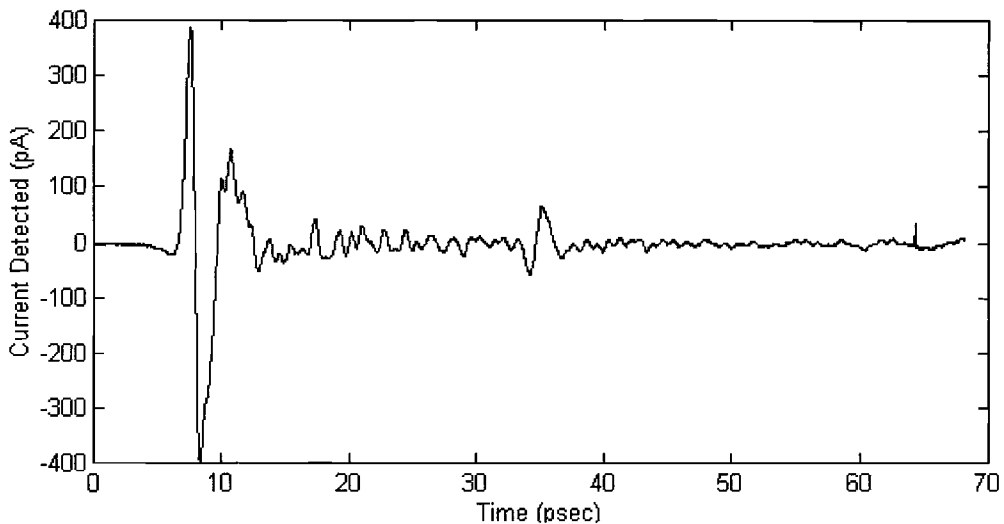


Figure 4-3) First backscattered THz signal received with 5.1 cm diameter mirror target located at 12 cm.

The minimum-to-maximum separation for this received pulse is 800 fsec. The maximum amount of current detected was ~ 400 pA. This is down from the ~ 900 pA received with no reflection into the enclosure. Note that the secondary pulse discussed earlier can still be seen at ~ 35 psec. Figure 4-4 contains the numerical Fourier transform of the first backscattered signal shown in Figure 4-3.

As mentioned, the oscillatory nature of the relative amplitude in Figure 4-4 can be attributed in part to the presence of a secondary pulse. Figure 4-4 shows that the first backscattered signal received has a center frequency of 300 GHz, a FWHM bandwidth of 370 GHz, and frequency components present above 1 THz.

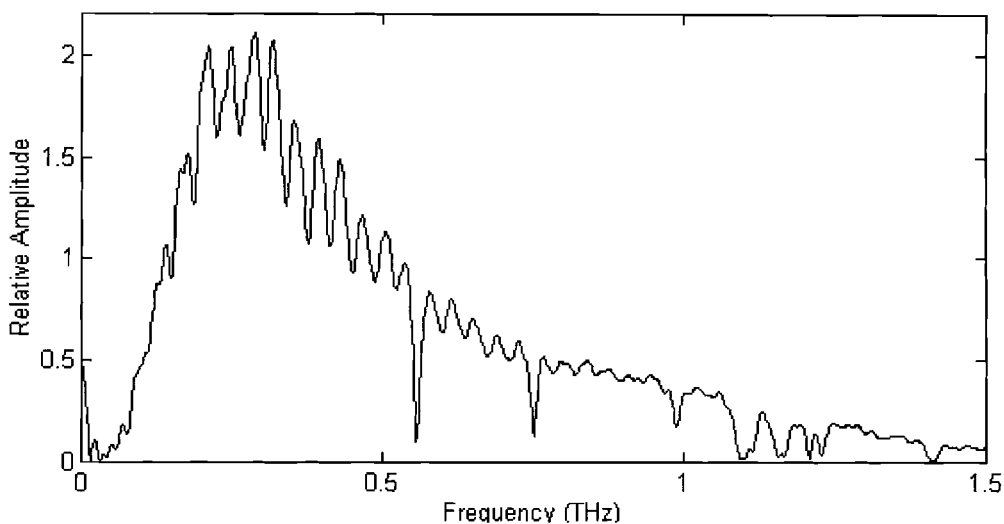


Figure 4-4) Frequency domain representation of Figure 4-3.

After receiving a reasonable signal from the 5.1 cm diameter mirror at 12 cm, the next logical step was to try a simple geometric object as a scattering target. The first such object was a standard brass post--the type used to hold optical mounts--which was placed in a 5.1 cm tall base and placed approximately where the mirror had been for the previous run. The diameter of the brass post was 13.7 mm.

In attempting to locate the returned pulse, the delay line was manually scanned around the point that the pulse was expected, a signal with a 35 pA maximum strength was found. Figures 4-4 and 4-5 show this detected signal in the time and frequency domains. In Figure 4-5 the minimum-to-maximum separation is 1.25 psec. A secondary pulse can still be seen at approximately 42 psec.

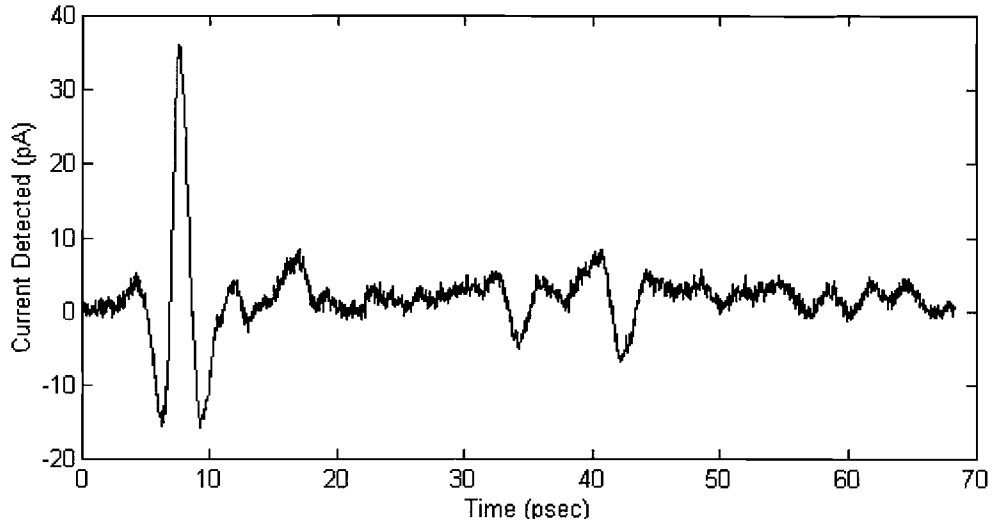


Figure 4-5) First backscattered THz signal received with a simple geometric object target (vertical cylindrical rod) located at 12 cm.

The numerical Fourier transforms of the mirror and brass rod scans, Figures 4-4 and 4-6 respectively, show that the spectrum changes considerably for the brass rod. The

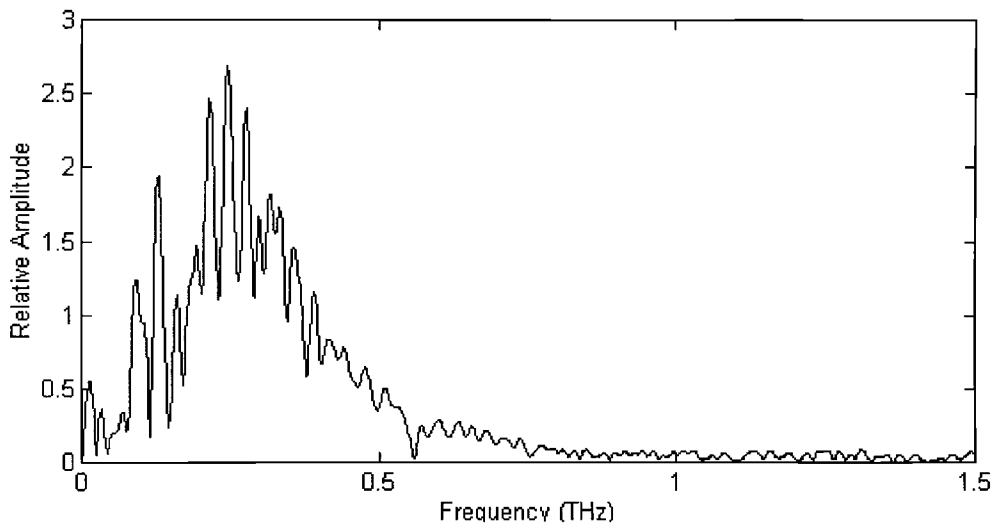


Figure 4-6) Numerical Fourier transform of Figure 4-5.

signal returned off of the brass rod seems to be "noisier" in the low frequency portion and exhibits lower magnitude components in the higher frequency range.

As mentioned, for the cylinder the time domain signal strength dropped to 35 pA from the 375 pA found with the 5.1 cm diameter Al coated mirror. This was expected as the cylindrical surface of the brass post spreads the returned radiation over an angle of approximately 180° while the second redirecting mirror subtends approximately 10° . If, for rough approximation, you assume that the THz radiation is spread evenly, around 6% of the reflected beam will be detected. This would correspond to approximately 22.5 pA of the original 375 pA. This appears to be a reasonable assumption.

The brass rod and holder were removed to determine if any of the detected signal was due to reflections from anything other than the intended target.

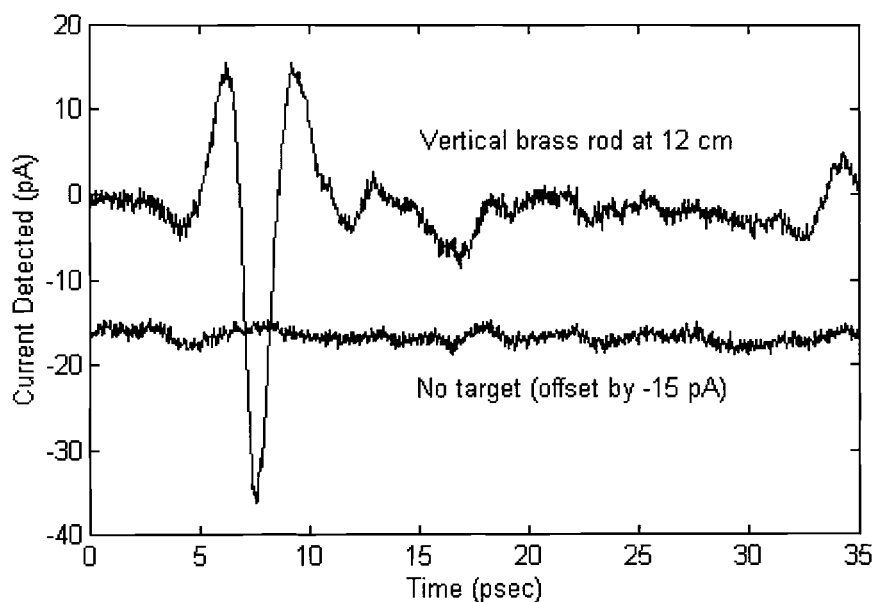


Figure 4-7) Determining contribution of unintended objects to overall signal received. The data obtained without a target has been offset by -15 pA for convenience.

In Figure 4-7, the scan taken without the target clearly shows that no significant signal was being returned when no target was present.

First Signals Obtained From Targets at ~1 Meter

Having detected a target at 12 cm, efforts were focused on detecting a target at a greater distance. A distance of ~1 meter was determined to be reasonable. The first target in this range to be detected was the same 5.1 cm diameter Al coated mirror. It was located 98 cm from both redirecting mirrors and on approximately the same horizontal plane as the transmitter/receiver apparatus. The peak signal strength in Figure 4-8 corresponds to approximately 105 pA.

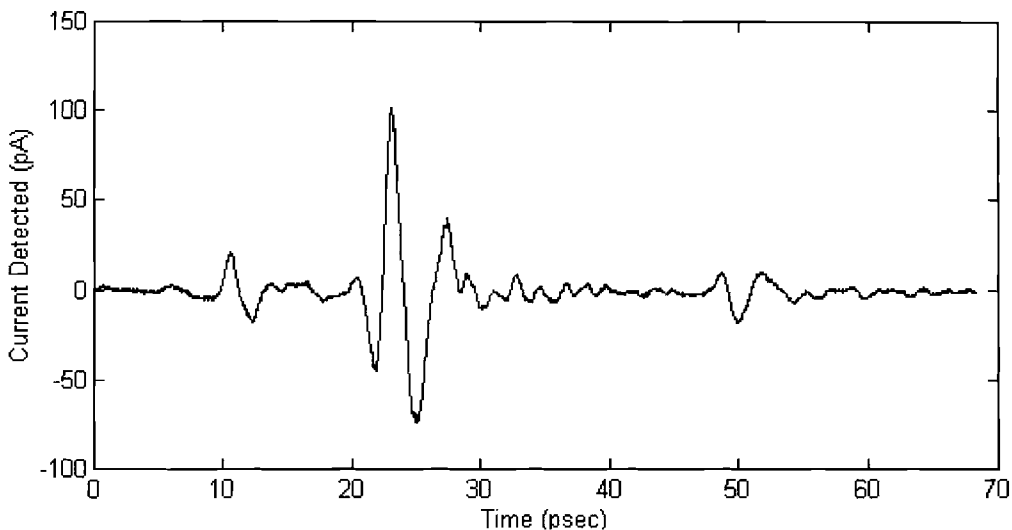


Figure 4-8) First backscattered THz signal received from a 5.1 cm diameter mirror at 98 cm.

Plainly visible in Figure 4-8 are small pulses at ~10 psec and ~50 psec. These are due to the "ghost" pulse train identified earlier in this chapter. The minimum-to-maximum separation is 2 psec for the pulse of interest, the larger magnitude pulse beginning at ~20 psec. This would suggest that some of the higher frequency components are being lost. This is supported by observing the numerical Fourier transform of this signal shown below in Figure 4-9.

As can be seen in the time and frequency domain representations (Figures 4-8 & 4-9), the presence of the "ghost" pulse train is contributing to the obtained results.

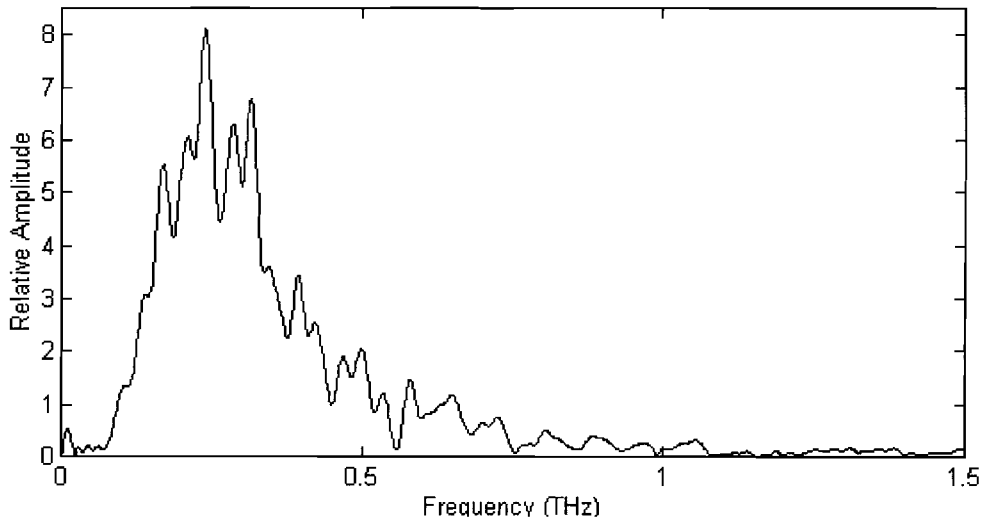


Figure 4-9) Numerical Fourier transform of Figure 4-8.

With the 5.1 cm diameter mirror as a reference, the same brass rod as that used in experimentation at 12 cm was placed so that its leading edge approximately coincided with the previous position of the leading edge of the mirror. A signal was obtained for the vertically oriented brass rod and is shown below in Figure 4-10.

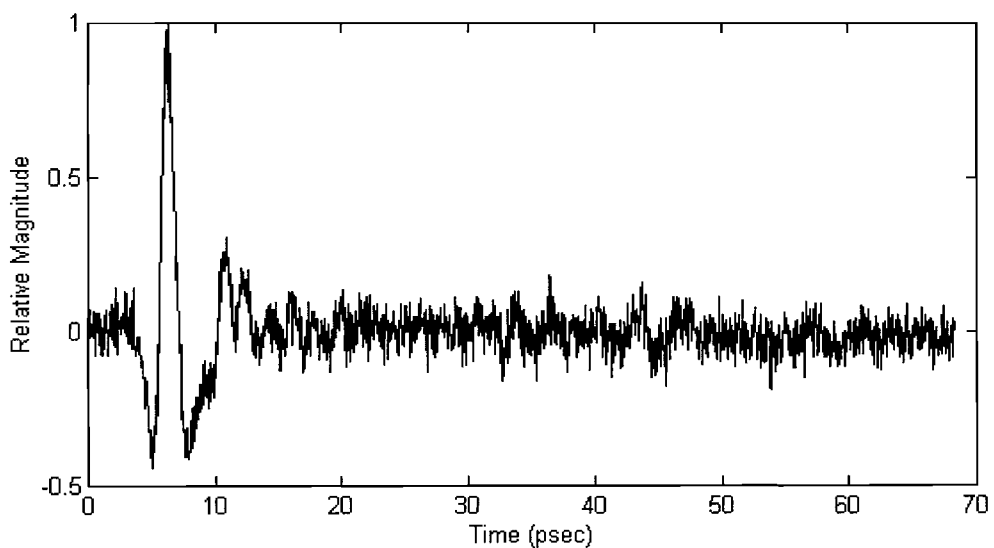


Figure 4-10) Backscattered THz signal received from a vertical brass rod at 98 cm.

It can be seen in Figure 4-10 that the minimum-to-maximum separation of the signal obtained is 1.25 psec. Figure 4-10 indicates that the vertical axis represents relative magnitude. This was necessary due to a discrepancy in the recorded full scale voltage for this measurement. Of importance is the general pulse shape observed and its magnitude relative to the noise present in the measurement.

Secondary pulses observable in other figures disappear into noise in Figure 4-10. The numerical Fourier transform for this signal is presented in Figure 4-11.

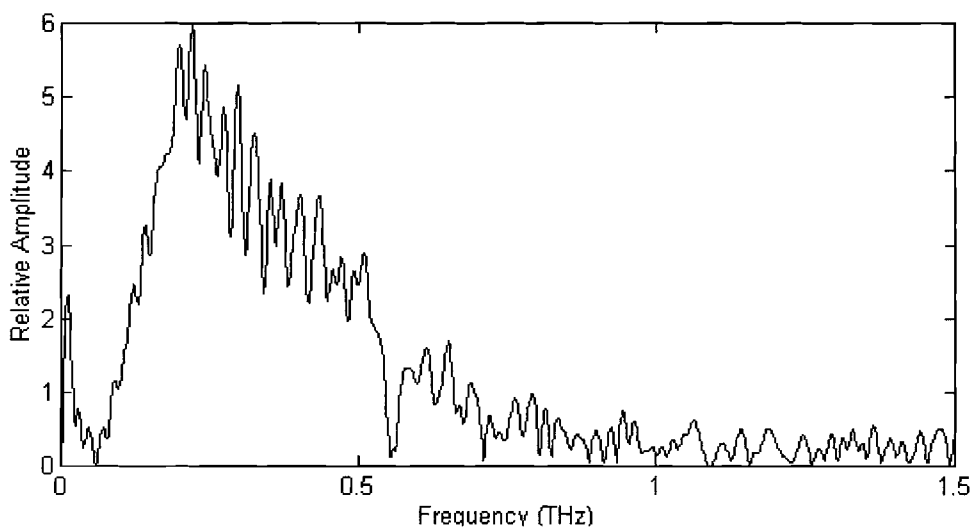


Figure 4-11) Numerical Fourier transform of Figure 4-10.

Figure 4-11 illustrates that frequency components are present to slightly above .5 THz. As with other signals obtained, water vapor absorption lines are clearly evident in the frequency domain.

Retuning System and Detecting Smaller Targets

Having obtained a valid signal from a vertically oriented cylindrical target located at ~1 meter, the next logical step was to try targets with smaller diameters. While doing this, several attempts were made to reduce a high amount of system noise. As explained in Chapter 2, a new mount was built for holding the target. In attempting to reduce the

system noise, the system was retuned with no reflection into the enclosure. This was accompanied by an increase in the beam power supplied to the chips. Initially, the laser beam power was measured before the final two steering mirrors. Upon measuring beam power closer to the chip, it was found that the power of the beam applied to the chip was below 20 mW. The variable beam splitter was adjusted to bring the delivered power up to the 20 mW desired.

The resulting signal obtained with no reflection into the enclosure is shown below in Figure 4-12.

The peak current is ~ 3 nA and the minimum-to-maximum separation is 1.2 psec. The detected current is a significant improvement over the first detected signal of Figure 4-1 which had a peak detected current of 900 pA.

The numerical Fourier transform of the new stronger signal is shown in Figure 4-13. It can be seen in comparing this to the spectrum of the first detected signal, Figure 4-1, that the spectrum is much "cleaner" for the new setup.

Another change was the replacement of the original 5.1 cm diameter Al coated mirror with a 10.2 cm square Al coated mirror to obtain a better reference signal.

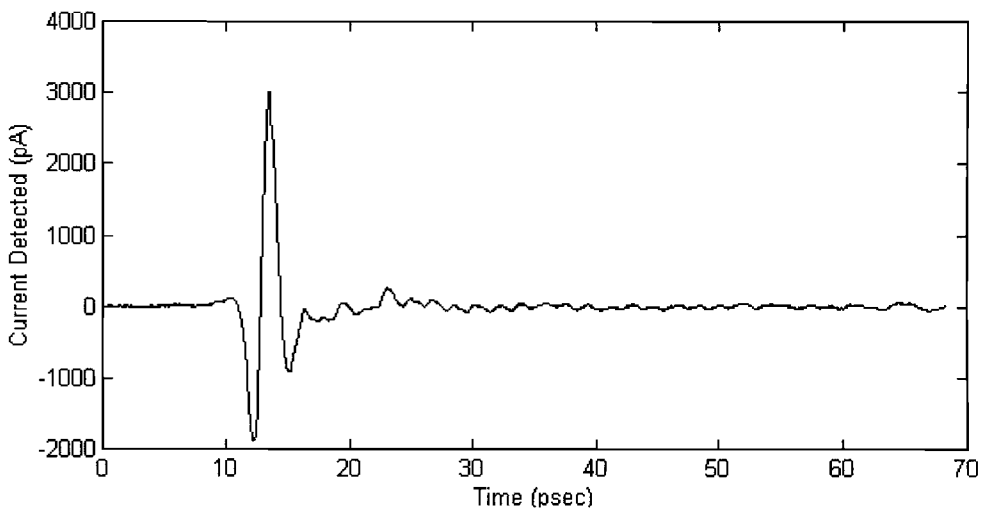


Figure 4-12) Best signal received with no redirection of THz beam into the enclosure.

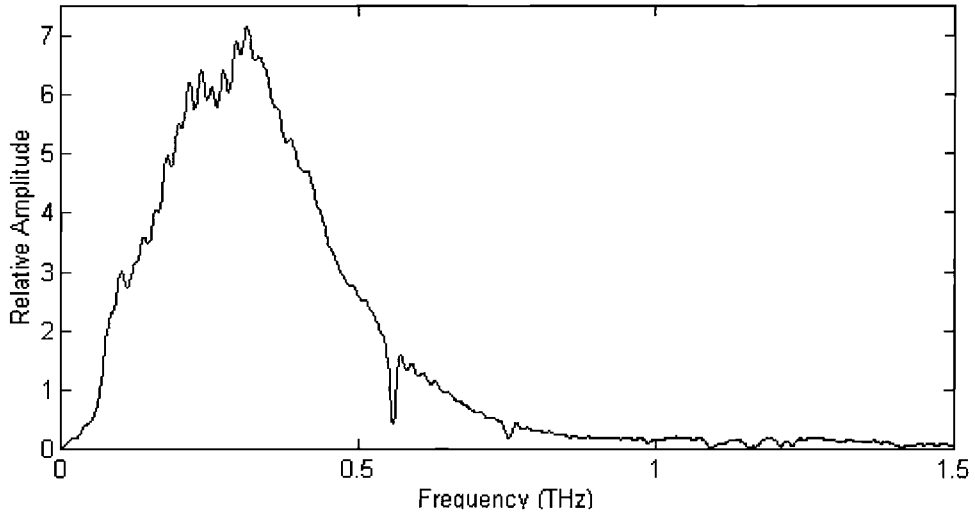


Figure 4-13) Numerical Fourier transform of Figure 4-12.

The best signal obtained with this square mirror is shown below in Figures 4-14 and 4-15. The peak current detected was on the order of 1.6 nA with a minimum-to-maximum separation of 1.5 psec. The secondary pulses present in earlier received signals are still present; however, their amplitudes relative to the main pulse decreased.

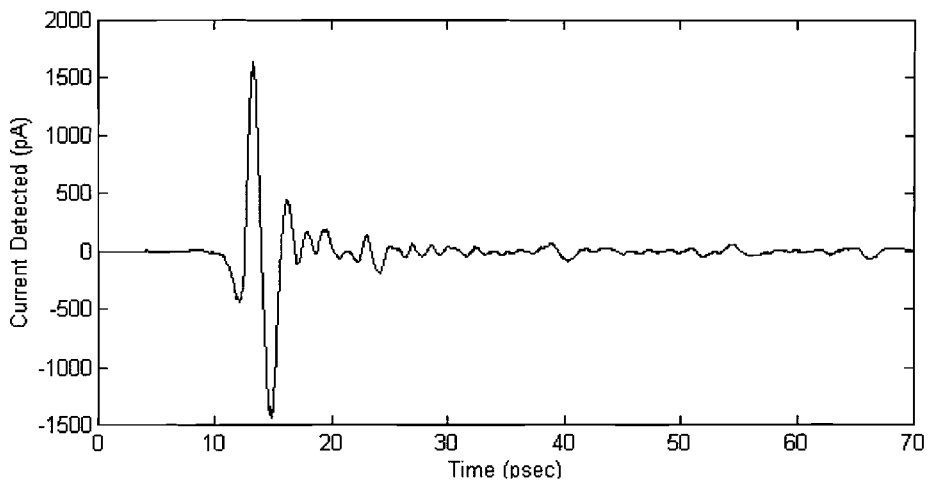


Figure 4-14) "Cleaner" signal obtained after peaking system, redesigning target mount, and changing target mirror to a 10.2 cm square mirror.

It can be seen in Figure 4-15 that the detected signal has a center frequency of 320 GHz, a FWHM bandwidth of 280 GHz, and components at frequencies as high as .8 THz.

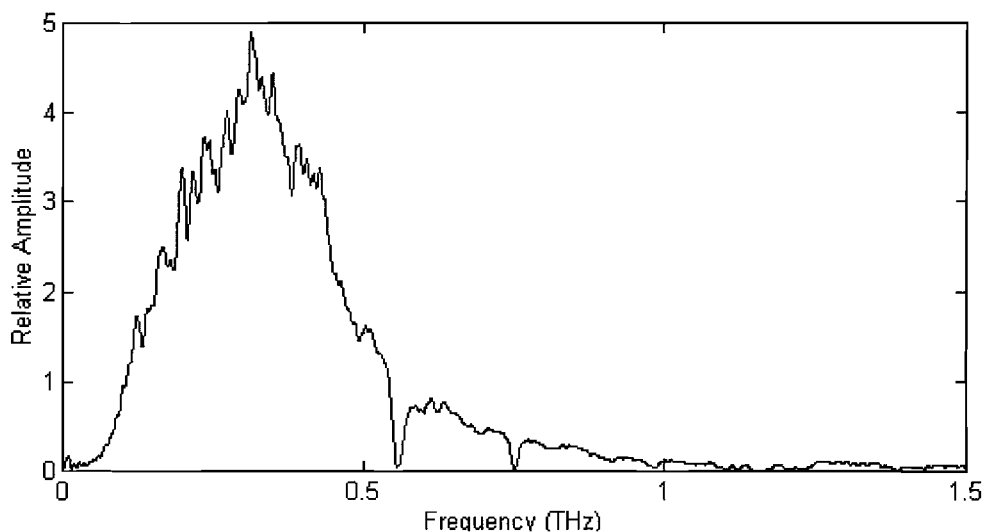


Figure 4-15) Numerical Fourier transform of Figure 4-14.

The retuned system made it possible to observe smaller targets at 1 meter due to increased signal strength. The magnitude of the desired pulse increased in relation to the magnitude of the secondary pulses present throughout this phase of research. Eventually, the smallest diameter vertically oriented cylindrical target that was detectable, without further elimination of system noise, was a length of 18 AWG (1.02 mm) uninsulated copper wire.

The Effect of Humidity

To study the effects of purging (filling the ranging enclosure with very low humidity air) on this particular setup, consecutive scans were taken at differing humidity levels. The target used for these scans was a 10.2 cm square Al coated mirror located 98 cm from the redirecting mirrors shown in Figure 2-1. The first scan was done at 58% relative humidity. Succeeding scans were taken while the water vapor level was changing. The second scan was taken with relative humidity varying between 31% at the

beginning of the scan and 26.5% by the end of the scan. Likewise, the humidity level during the third scan ranged from 26.5% to 23.5% while it ranged from 53% to 57% for the final scan.

It can be seen by observing the time domain data (Figure 4-16) that the late time response loses much of its oscillatory characteristics with decreasing water-vapor levels and indeed the entire received signal appears much "smoother." This is illustrated in Figure 4-16 below, which is a close look at the differing responses between 18 and 29 psec. The dotted ellipse indicates the region of interest.

Most of the data gathered during this investigation was taken without any purging of the enclosure. The laboratory was usually between 58% and 60% relative humidity. As a result, the first three vapor lines indicated in Table 2-1 are easily observable in the experimental data obtained. In addition, the rapid oscillatory nature of the late time response of the received THz signals can be attributed--at least partially--to the effects of water vapor.

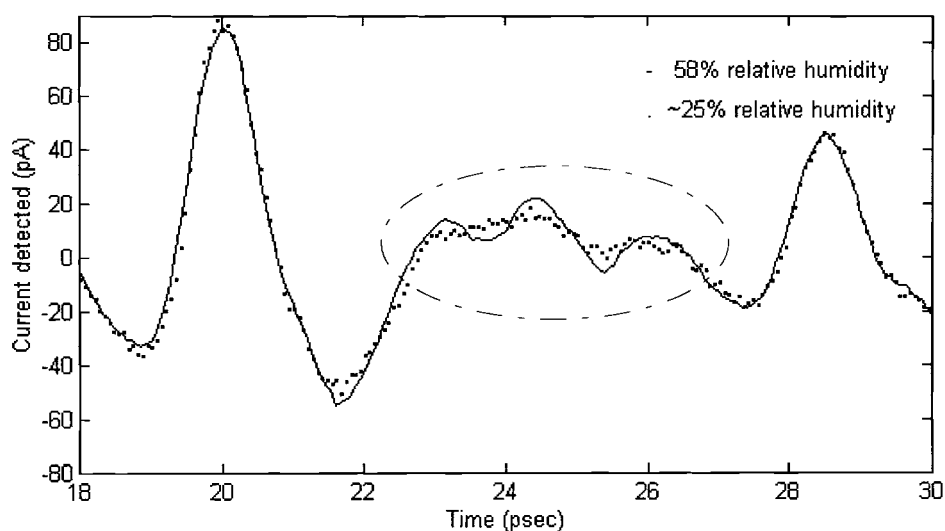


Figure 4-16) The elliptical area illustrates the "smoother" late time response associated with lower humidity in the enclosure.

By looking at the time domain results in Figure 4-16, it becomes clear that purging the ranging enclosure is not necessary for observing general pulse shapes. The shape and magnitude of the prominent features of the detected signal remain the same with changing water vapor levels. As the thrust of this experiment was simply to explore the possibility of using this technology at a distance up to 1 meter, the enclosure was not purged for most of the experimental run. "Cleaner" results could have been attained with constant purging; however, this would have taken a significant amount of additional time for each measurement.

Maximum Detected Backscattered Signals From Vertically Oriented Targets

The best results obtained are shown below with appropriate Fourier transforms. Figures 4-17 and 4-18 represent the best signal obtained from a 13.7 mm diameter vertically oriented brass rod located 1 meter from the redirecting mirrors.

The minimum-to-maximum separation for the returned pulse in Figure 4-17 is 1.11 psec. The maximum current detected was 78 pA.

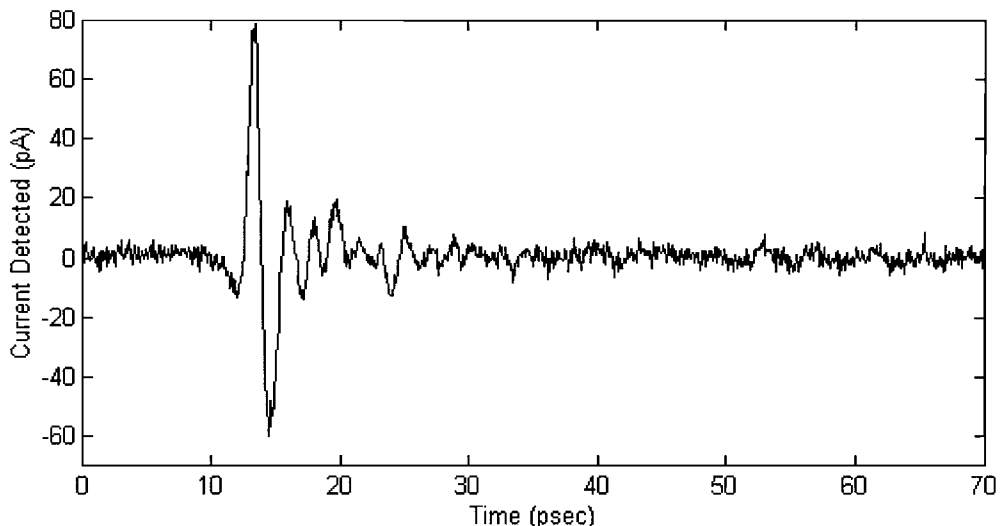


Figure 4-17) Best signal received with vertically oriented 13.7 mm diameter brass rod at 1 meter.

Figure 4-18 demonstrates that frequency components were present at frequencies up to ~ 0.75 THz. The stronger signal obtained (Figure 4-17) results in a "cleaner" spectrum. This can be verified by comparing the frequency domain representations of the signals received before and after retuning the system, Figure 4-11 and Figure 4-18 respectively.

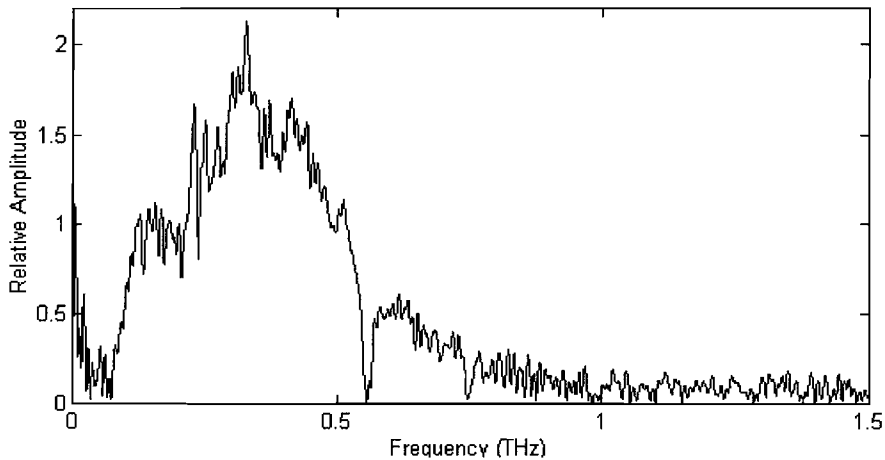


Figure 4-18) Numerical Fourier transform of Figure 4-17.

In Figures 4-19 and 4-20 are the time and frequency domain representations of the

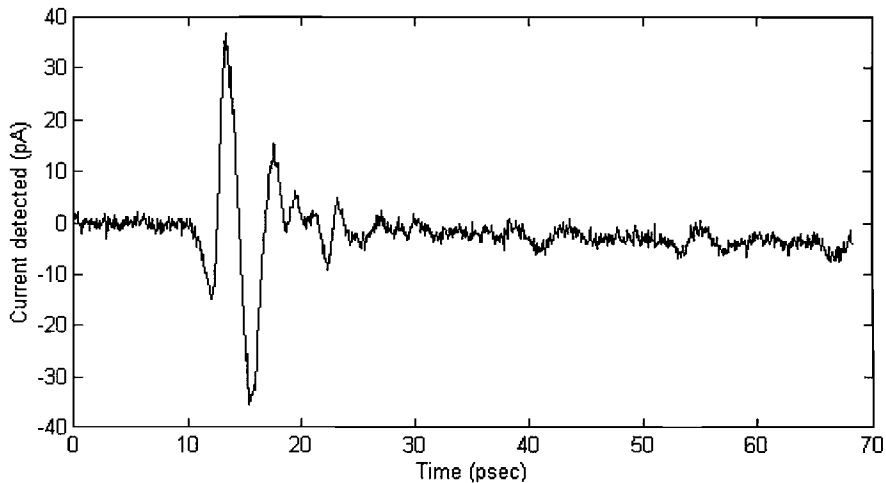


Figure 4-19) Best signal received with vertically oriented 6.4 mm diameter copper tubing at 1 meter.

signal received from a length of 1/4" (6.35 mm) outer diameter copper tubing at 1 meter. Figure 4-19 indicates a peak detected current of 37 pA.

Figure 4-20 reveals that frequency components up to ~ 0.6 THz are present in the pulse returned from the 6.4 mm diameter copper tubing.

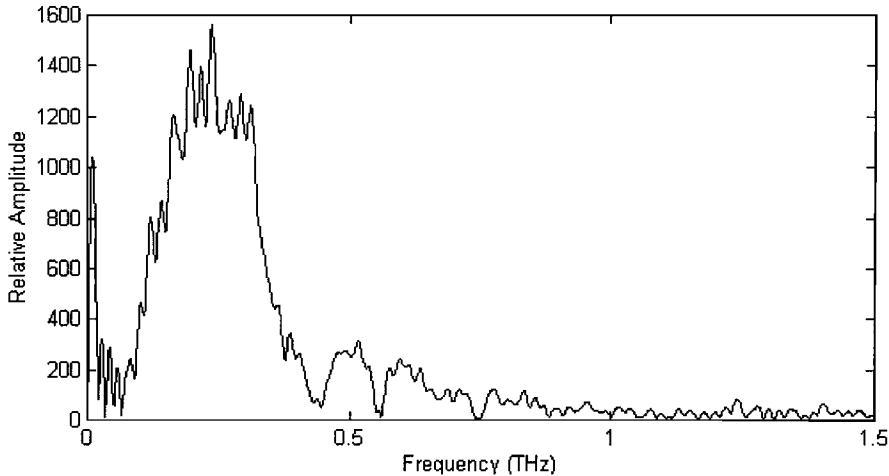


Figure 4-20) Numerical Fourier transform of Figure 4-19.

Figures 4-21 and 4-22 show the signal received from a length of 1/8" (3.17 mm) outer diameter copper tubing at 1 meter.

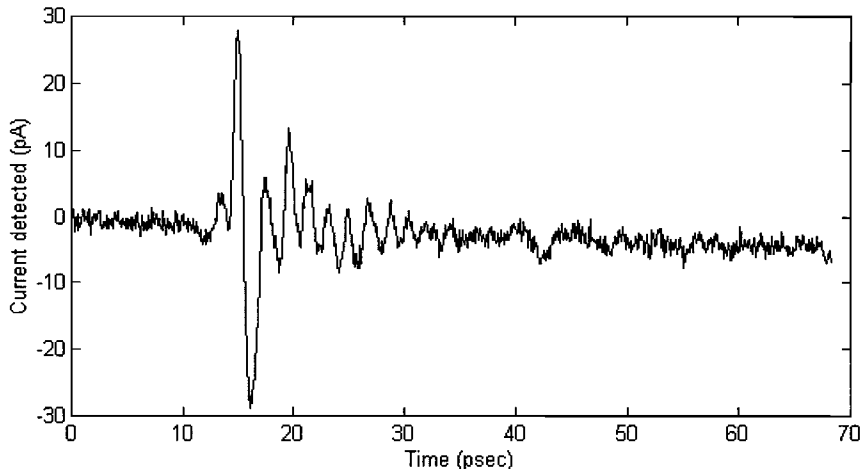


Figure 4-21) Best signal received with vertically oriented 3.2 mm diameter copper tubing at 1 meter.

In Figure 4-21, the maximum current detected was 28 pA while the minimum-to-maximum separation for the pulse was 2.3 psec. The late time response extends beyond 30 psec for this 3.2 mm outer diameter copper tubing. Figure 4-22 represents the numerical Fourier transform for the 3.2 mm copper tubing. Frequency components exist in Figure 4-22 up to ~ 0.8 THz.

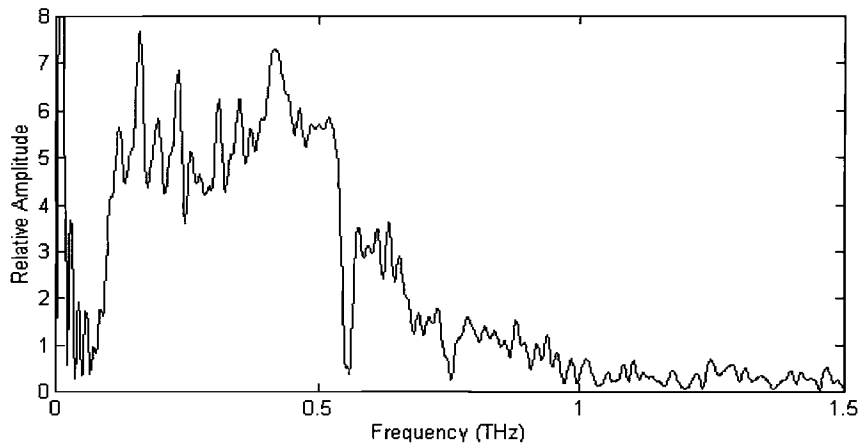


Figure 4-22) Numerical Fourier transform of Figure 4-21.

Finally, Figures 4-23 and 4-24 represent the results obtained from a length of 18 AWG (1.02 mm) copper wire at 1 meter.

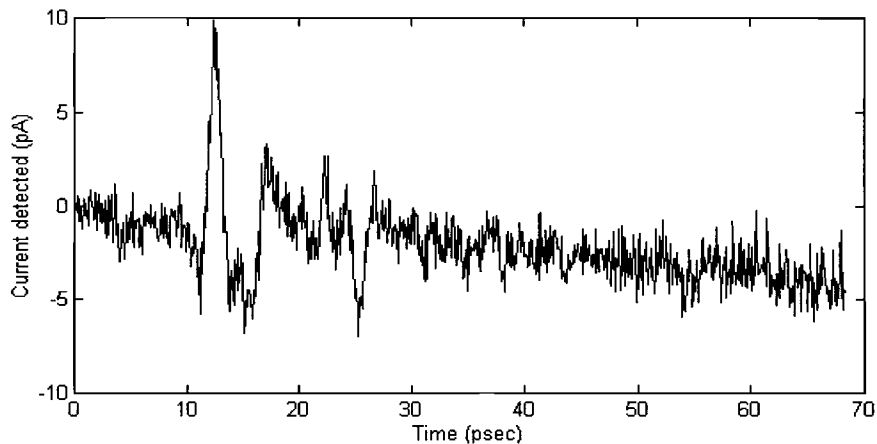


Figure 4-23) Best signal received with vertically oriented 1.0 mm diameter copper wire at 1 meter.

It can be seen by inspection that the peak detected current for the 1.0 mm diameter copper wire was approximately 9 pA. This was the smallest signal observable above the 2 pA of noise present in the measurement. For this signal, the minimum-to-maximum separation is difficult to measure accurately due to noise. The separation was between 1.7 and 2.0 pA.

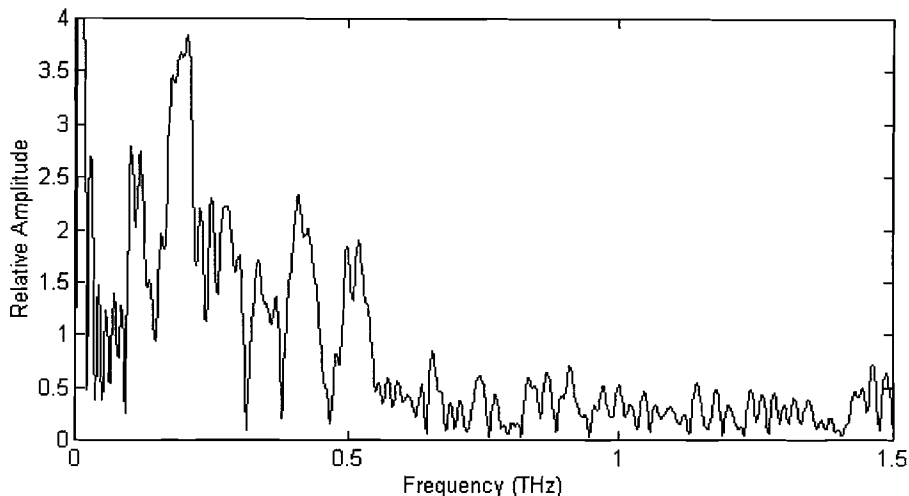


Figure 4-24) Numerical Fourier transform of Figure 4-23.

The numerical Fourier transform shown in Figure 4-24 gives little useable information. This is due to low signal-to-noise ratio present in the returned signal for this 1.0 mm diameter copper wire.

Summary of Results With Vertically Oriented Cylindrical Targets

The capabilities of this THz system can be observed in the above plots. Using vertically oriented cylindrical targets and gradually reducing the target's diameter resulted in the returned signal disappearing into the background noise for diameters less than 1.0 mm. The maximum signal obtained for the 1.0 mm diameter wire corresponds to a detected current of approximately 9 pA. This is down from the 78 pA signal obtained with a 13.7 mm diameter brass rod. In Figure 4-23 it can be seen by inspection that the

It can be seen by inspection that the peak detected current for the 1.0 mm diameter copper wire was approximately 9 pA. This was the smallest signal observable above the 2 pA of noise present in the measurement. For this signal, the minimum-to-maximum separation is difficult to measure accurately due to noise. The separation was between 1.7 and 2.0 pA.

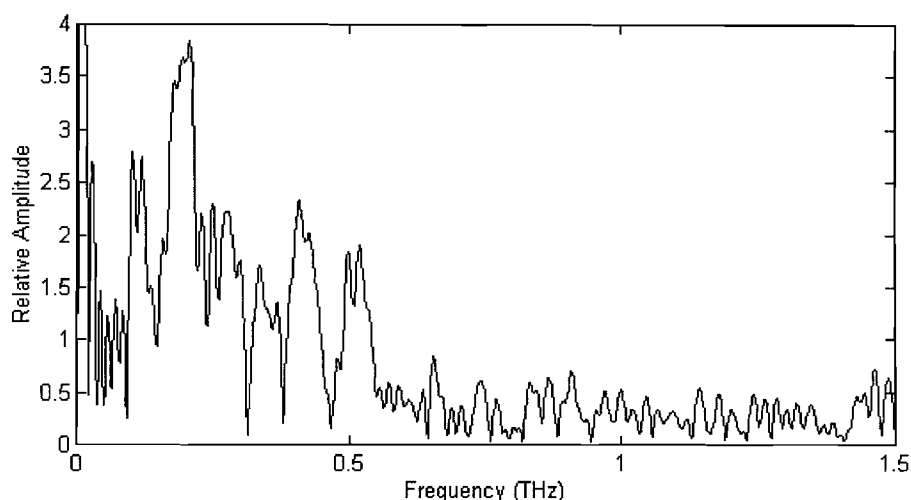


Figure 4-24) Numerical Fourier transform of Figure 4-23.

The numerical Fourier transform shown in Figure 4-24 gives little useable information. This is due to low signal-to-noise ratio present in the returned signal for this 1.0 mm diameter copper wire.

Summary of Results With Vertically Oriented Cylindrical Targets

The capabilities of this THz system can be observed in the above plots. Using vertically oriented cylindrical targets and gradually reducing the target's diameter resulted in the returned signal disappearing into the background noise for diameters less than 1.0 mm. The maximum signal obtained for the 1.0 mm diameter wire corresponds to a detected current of approximately 9 pA. This is down from the 78 pA signal obtained with a 13.7 mm diameter brass rod. In Figure 4-23 it can be seen by inspection that the

noise present corresponds to a current of approximately 2 pA. The following plot overlays the above results for comparison of relative amplitudes.

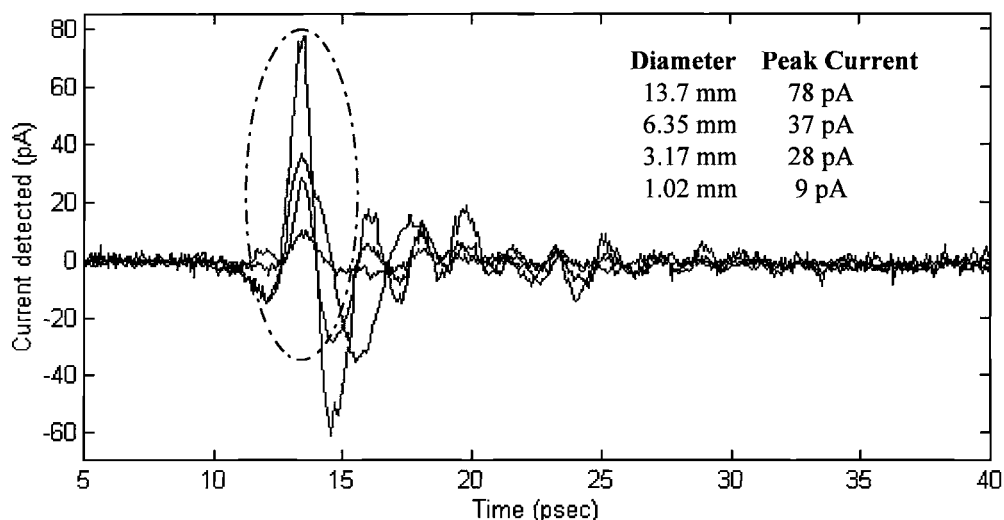


Figure 4-25) Comparison of detected signal strength for vertically oriented cylindrical targets of varying diameters located at 1 meter.

Observing the amplitudes of the peaks located within the elliptical area in the above figure shows that the strength of the returned signal varies almost linearly with the diameter of the target. This is shown in the Figure 4-26 below.

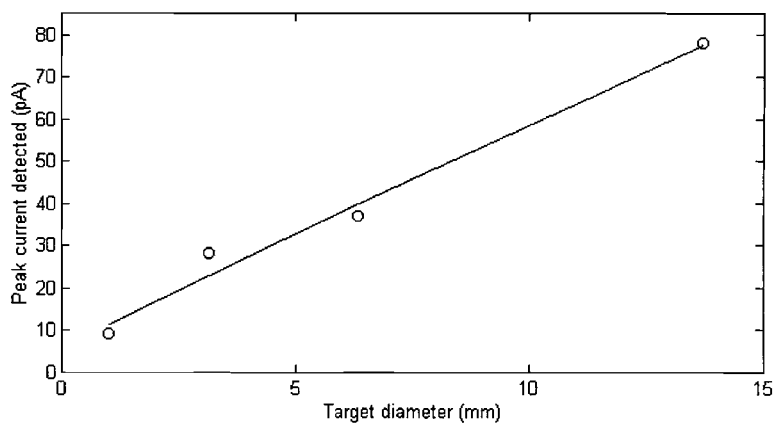


Figure 4-26) Dependence of peak detected current on vertically oriented cylindrical target's diameter.

All targets shown were located at the same distance (100 cm) from the redirecting mirrors. Also plainly visible is the trend of the signal disappearing into the noise level with diameter below 1.0 mm.

Detection of vertical cylindrical targets with diameters smaller than 1.0 mm require increased signal to noise ratios. Reducing the unusually high system noise would have the desired effect. Although not realized in this phase of research, a typical signal to noise ratio for this type of system is 10,000:1.¹

The Effect of Target Orientation

Another step in this investigation was to determine the dependence of received signal strength on the physical orientation of the target. Since the coplanar transmission lines on the transmitting antenna are vertically oriented, the bursts of THz radiation created have an E-field polarized in the horizontal plane. The receiver must be oriented similar to the transmitter for detection of the incoming THz signal. To determine the effect of this E-field polarization on the signal returned from a target, a mount was fabricated to orient the same 13.7 mm brass rod in the horizontal plane. A scan was taken with this configuration and is shown below in Figure 4-27.

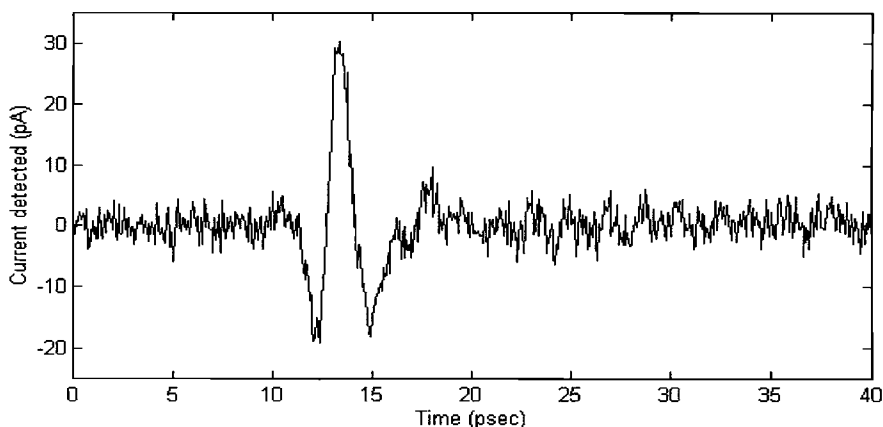


Figure 4-27) Determination of the effect of target orientation on returned signal using horizontally oriented 13.7 mm diameter brass rod at 1 meter.

The peak current detected was on the order of 30 pA with a minimum-to-maximum separation of 1.1 psec. This scan was taken before the retuning of the system mentioned earlier. Under similar conditions, the peak current detected was on the order of 20 pA. Comparing the amount of current detected with the horizontally oriented brass rod to that detected with the vertically oriented brass rod shows a 10 pA increase in signal strength. This dependence on the physical orientation of the target was identified as an area for future investigation. For this diameter of target, the signals obtained are of the same order of magnitude.

It was difficult to make fine adjustments to the rotational position of the horizontal rod; therefore, better results could have been attained with more precise adjustment of the rod's angle in relation to the incoming beam. Given the approximate equivalence in signal strength, the cylindrical targets used in the remainder of this investigation were oriented vertically.

Collimation Study

Having a nonuniform beam results in the frequency content of the backscatter received from a given target being dependent upon the target's positioning within the beam.

To investigate this, a target located at 100 cm was translated from the center of the beam to the extreme edge of the beam in incremental steps on successive scans. The signals detected on these successive scans are plotted on a common time axis in Figure 4-28 below. It can be seen by inspection that the returned pulse shape varies as the target is translated across the THz beam.

In Figure 4-29 the numerical Fourier transforms of the data points obtained for no horizontal shift and for a 17 mm shift are plotted on a common frequency axis.

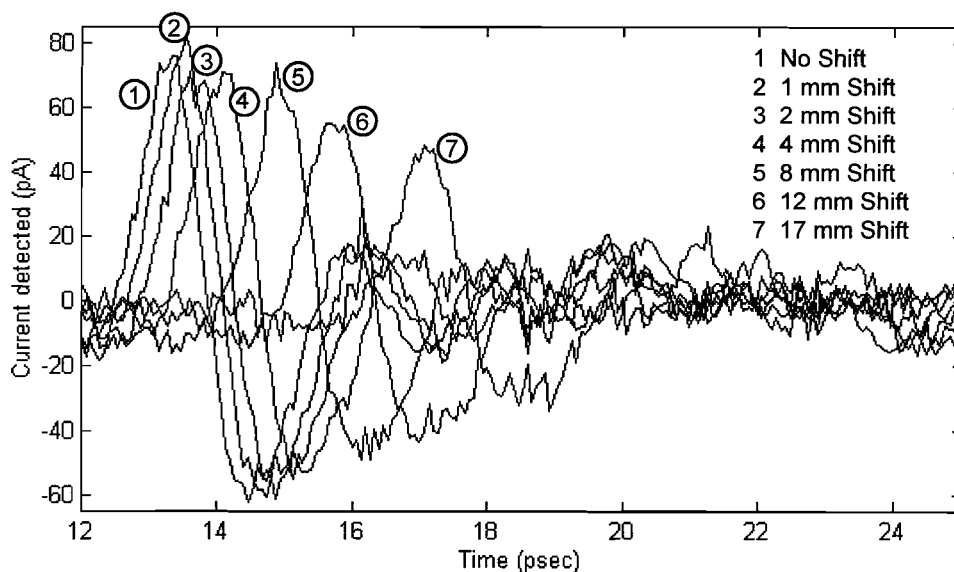


Figure 4-28) Shifting target to determine frequency distribution within THz beam

Examination of Figure 4-29 reveals that the frequency components are of smaller magnitude in the range from about 300 GHz to 600 GHz. This change in the spectrum as the target is horizontally translated suggests that the higher frequency components are located in the center of the THz beam.

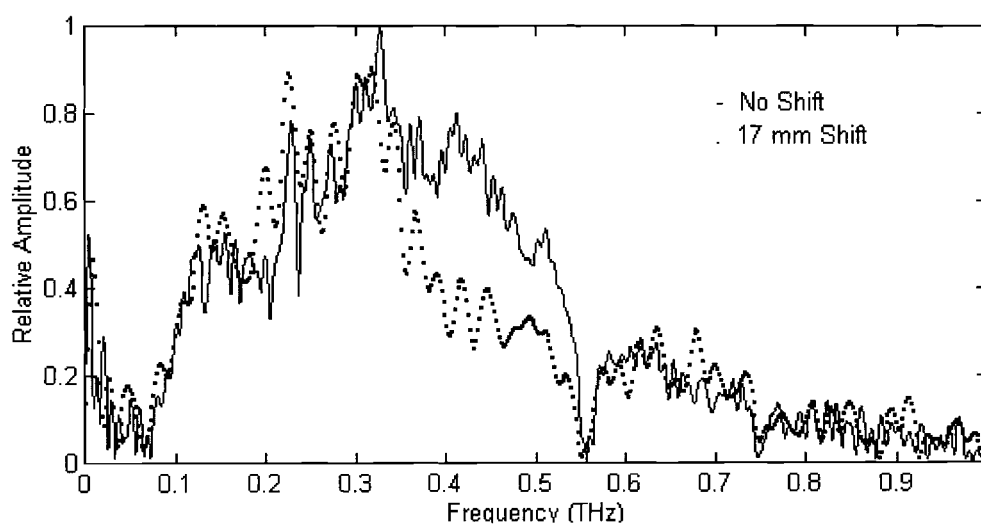


Figure 4-29) Comparison of spectrum for target centered in THz beam and shifted 17 mm perpendicular to beam path.

The time domain and frequency domain representations of these data sets demonstrate that the assumption that the frequency content of the backscattered signal is dependent upon the positioning of the target within the beam is valid.

Once a signal was obtained with a 5.1 cm diameter mirror at 98 cm, apertures were used to determine the location of the THz beam. Once the beam was located, the strength of the received signal was observed as the diameter of the aperture was reduced. The results are tabulated in Table 4-1.

Table 4-1) Determining THz beam collimation

Distance from Mirror	Full Width Half Maximum
165 mm from 1 st paraboloidal mirror	17 mm
Close to 5.1 cm diameter target mirror	~20 mm (very rough)
165 mm from 2 nd paraboloidal mirror	17 mm
At 2 nd paraboloidal mirror	16 mm

The values given for Full Width Half Maximum (FWHM) correspond to the aperture size at which the received signal strength was reduced by 50%. The measurement taken close to the target is annotated as being a very rough measurement. This is due to the aperture housing interfering with the outgoing beam when measuring the incoming beam and vice versa. For all other measurements taken, this was not a problem.

It can be seen that the THz beam is very well collimated over the entire path of propagation. The beam profile can be approximated fairly well by assuming a Gaussian distribution of power.

Results Obtained With a Spherical Target

Having investigated the use of this system for backscatter measurements using cylindrical targets, determining the performance of the system with a spherical target at 1 meter was evaluated. The target holder was modified to support a 2.5 cm diameter brass sphere. The sphere was held above the target mount by a small length of plastic tubing. As mentioned previously, the target mount allowed for adjustments in the vertical plane and in the horizontal plane perpendicular to the THz beam path.

A simplistic view of the backscattered signal from a spherical object gives some insight into the expected signal level. The scattering occurs in three dimensions instead of the approximate two dimensional scattering which occurs with normal incidence on a cylindrical object. If you assume that the signal is scattered over one hemisphere with a radius of 1 meter (surface area of 6.28 m^2) and that the 5.1 cm mirror has a surface area of 20.4 cm^2 you can see that only .03% of the transmitted signal would be incident upon the second redirecting mirror. Given the original signal strength of 1.6 nA (Figure 4-14), this .03% would correspond to .52 pA. The actual results obtained yielded a returned peak current detected ranging from 3 to 8 pA as shown in Figures 4-30 and 4-31. Therefore, an order of magnitude discrepancy exists between the detected and estimated signal strength. This can be attributed to the greater complexity of scattering in three dimensions.

The reflected ranging signal from the 2.5 cm diameter sphere was just observable above the noise level in the system. Shown in Figure 4-30 below is the time domain representation of the data taken for the spherical target at 1 meter. The peak detected current was approximately 8 pA with a minimum-to-maximum separation of ~1.5 psec.

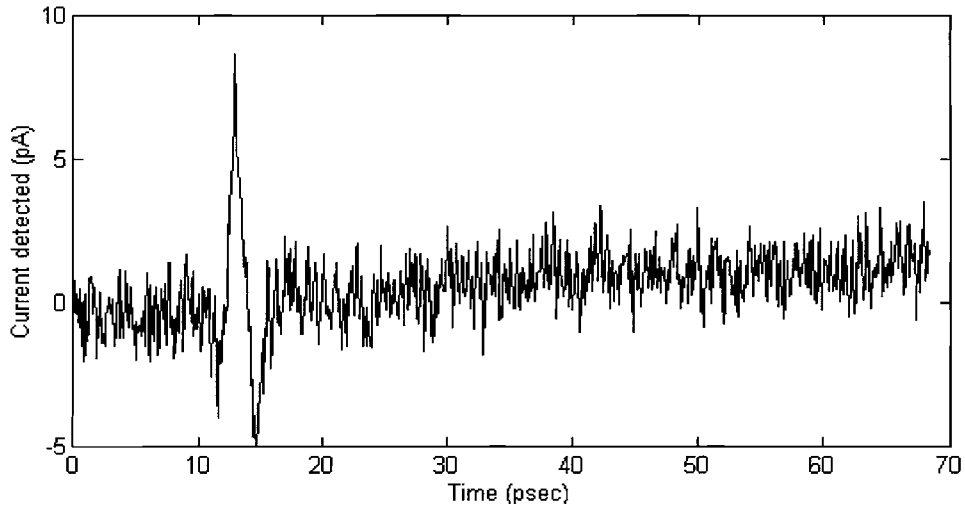


Figure 4-30) Signal detected using 2.5 cm diameter brass sphere at 1 meter.

A second data series was obtained for this target by taking four successive scans and averaging to help reduce the noise present in the received signal. This gave a much "clearer" picture of the received signal and is shown in Figure 4-31. The averaged measurement yielded a peak detected current of 3.2 pA. The minimum-to-maximum separation was the same as that found in Figure 4-30 (~1.5 psec).

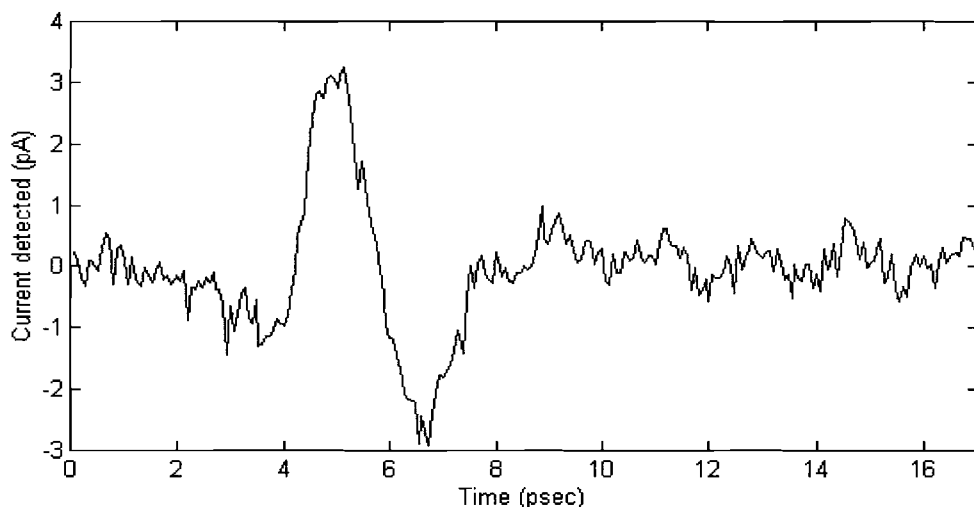


Figure 4-31) Numerical average of 4 data scans taken with 2.5 cm diameter brass sphere at 1 meter.

To compare the signals obtained with and without averaging, the measurements shown in Figures 4-30 and 4-31 are combined in Figure 4-32 below.

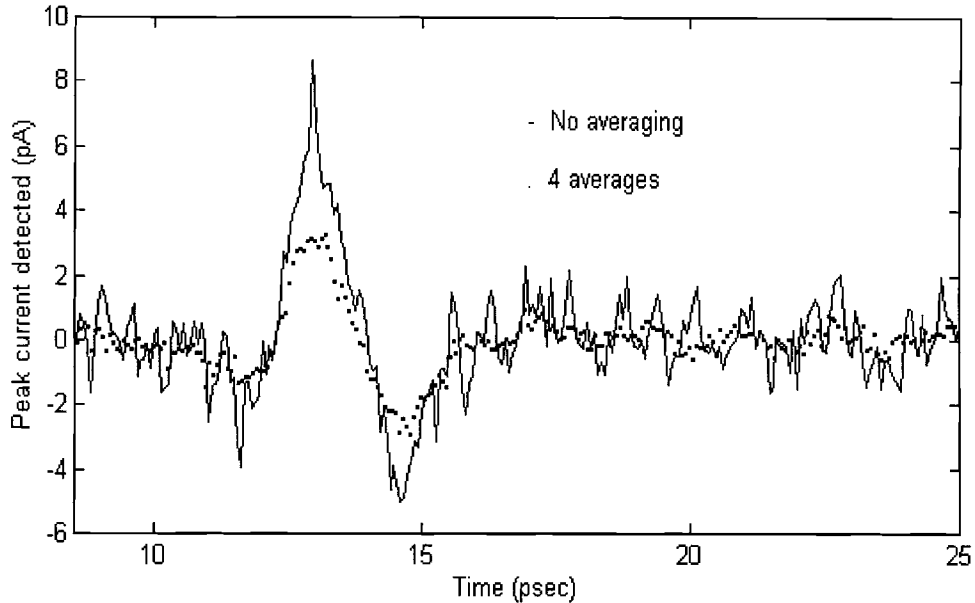


Figure 4-32) Comparison of signal detected with and without averaging using 2.5 cm diameter brass sphere at 1 meter.

Figure 4-32 illustrates that averaging does reduce the amount of noise seen in the measurement without affecting the general pulse shape observed. As mentioned, the minimum-to-maximum separation for both pulses is ~ 1.5 psec.

The numerical Fourier transform of the averaged signal in Figure 4-31 is shown in Figure 4-33. It can be seen by observation that frequency components exist at and above .5 THz. The spectrum appears much smoother than the other spectra appearing in this paper due to the averaging of the measurement and the reduced time window of the measurement.

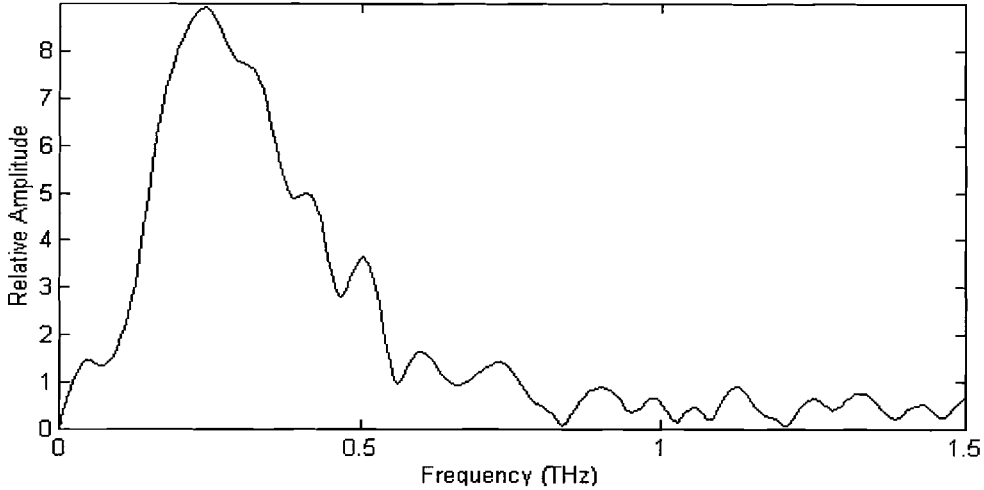


Figure 4-33) Numerical Fourier transform of Figure 4-31.

In Carin and Agi's paper⁴, a steel sphere with a diameter of 2.5 cm was used as a target. This sphere was located 7.0 cm from the transmitting antenna and 5.5 cm from the receiving antenna. In their setup, the angle between the transmitter and receiver was 75° .

Given that the highest frequency components in their experiment are around 70 GHz, the smallest wavelength present would be $\frac{c}{f} = \frac{2.998 \cdot 10^8 \text{ ms}^{-1}}{70 \cdot 10^9 \text{ s}^{-1}} = 4.28 \text{ mm}$. Considering this, the target was located ~ 16 wavelengths away from the transmitting antenna and ~ 13 wavelengths from the receiving antenna.

In this setup, the brass sphere was located 1 meter from both redirecting mirrors. The angle between the redirecting mirrors is very small ($\sim 2^\circ$). With the highest frequency components extending above .5 THz, the smallest wavelength component present was $\frac{c}{f} = \frac{2.998 \cdot 10^8 \text{ ms}^{-1}}{1.0 \cdot 10^{12} \text{ s}^{-1}} = 300 \mu\text{m}$. Since the target is equidistant from the transmitter and receiver redirecting mirrors, both transmitter and receiver are separated from the target by ~ 1700 wavelengths at .5 THz.

It can be seen that the target distance to wavelength ratio is over 100 times greater for this system operating around .5 THz (600 μm) than it was for Carin and Agi's system operating around 70 GHz (4.28 mm).

CHAPTER 5

CONCLUSIONS AND FUTURE RESEARCH

The purpose of this investigation was to perform a test of the feasibility of using this type of apparatus for performing ranging measurements. It was proven that it is possible to detect targets at distances of up to 1 meter. This is considerably longer than the previous target distance reported by Carin and Agi.⁴ The results presented in this paper are believed to be the first ranging measurements ever reported with a bandwidth extending over .5 THz. In this investigation, the smallest target used at 1 meter was a vertically oriented copper wire with a diameter of 1.0 mm. Before this investigation, the longest reported distance this type of measurement had been taken at was ~ 7.0 cm (16λ at 70 GHz) for a 2.5 cm diameter conducting sphere and ~ 12.5 cm (30λ at 70 GHz) for parallel 5 mm wide Aluminum strips.⁴

Current plans call for the elimination of the secondary pulse train identified in Chapter 4. This should drastically improve the received signals and allow for the observation of smaller targets.

As mentioned in the body of this report, the targets used for the bulk of the experimentation consisted of vertically oriented cylinders. These simple geometric objects lend themselves well to theoretical evaluation. Current plans call for a detailed comparison of received data to theoretical expectations. Using theoretical comparisons, an investigator should be able to differentiate between horizontally and vertically oriented targets.

It is planned to use the system developed for this investigation to study the backscattered signals from objects that are geometrically complex, such as scale model

aircraft. The ultra-wideband nature of the generated THz pulses should provide a large amount of information. The returned signal should contain features from submillimeter variations in the target surface. Considering that X band radar extends from 8 to 12 GHz and this system has frequency components present above .75 THz, the wavelengths present are roughly two orders of magnitude shorter for this system than for X band radar. This would enable utilization of models on the 1:72 scale in table top ranging with this system to represent accurate target to wavelength ratios.

An important result of this research is the demonstration of the ability to create a useable, tightly collimated, freely propagating beam of THz radiation which extended over an appreciable distance. Throughout most of the investigation, the total path length of the THz beam was over 2 meters. This was done through air with humidity levels on the order of 60%.

The possible uses of this THz system are numerous. During the course of this investigation, the need arose to determine the fast and slow axes of sapphire wafers being taken to IBM Watson Research Center for chip fabrication. (The birefringence of sapphire results in differing propagation speed depending on physical orientation.) This was accomplished by placing the wafer in question in the THz beam and determining the position of the detected pulses in time. The wafer was then rotated by 90° in the THz beam and the position of the detected pulse was again determined. Comparing these two measurements allowed for simple and accurate determination of the fast and slow axes of the sapphire wafer.

Another possible use of the system developed for this experiment is time-domain gas spectroscopy. The size of the airtight enclosure will provide a total path length of ~2 meters through the gas under investigation.

BIBLIOGRAPHY

- 1) M. van Exter and D. Grischkowsky, "Characterization of an optoelectronic terahertz beam system," *IEEE Transactions on Microwave Theory and Techniques*, vol. 14, p. 1684, 1989.
- 2) M. van Exter, Ch. Fattinger, and D. Grischkowsky, "Terahertz time-domain spectroscopy of water vapor," *Optics Letters*, vol. 14, p. 1128, 1989.
- 3) D. Grischkowsky, Soren Keiding, M. van Exter, and Ch. Fattinger, "Far-infrared time-domain spectroscopy with terahertz beams of dielectrics and semiconductors," *J. Opt. Soc. Am. B*, vol. 7, p. 2006, 1990.
- 4) L. Carin and K. Agi, "Ultra-wideband transient microwave scattering measurements using optoelectronically switched antenna," *IEEE Transactions on Microwave Theory and Techniques*, vol. 41, p. 250, 1993.
- 5) D. Kralj and L. Carin, "Short-pulse scattering measurements from dielectric spheres using photoconductively switched antennas," *Applied Physics Letters*, vol. 62, p. 1301, 1993.
- 6) A. Rahman, D. Kralj, L. Carin, M. Melloch, and J. Woodal, "Photoconductively switched antennas for measuring target resonances," *Applied Physics Letters*, vol. 64, p. 2178, 1994.
- 7) N. Katzenellenbogen and D. Grischkowsky, "An ultra-wideband optoelectronic THz beam system," *Ultra-Wideband, Short-Pulse Electromagnetics*, Edited by H. Bertoni *et al.*, Plenum Press, 1993.
- 8) K. Sam Shanmugan and A.M. Breipohl, *Random Signals*, New York: John Wiley and Sons, 1988.

VITA

Bradley W. Nicholson

Candidate for the Degree of

Master of Science

Thesis: RANGING STUDIES WITH AN ULTRA-WIDEBAND, PULSED,
OPTOELECTRONIC THz BEAM SYSTEM

Major Field: Electrical Engineering

Biographical:

Personal Data: Born in Ballwin, Missouri, on December 27, 1968. Son of Michael Nicholson and Joyce Cremer.

Education: Received Bachelor of Science degree in Electrical Engineering from the University of Missouri-Rolla in 1992. Completed the requirements for the Master of Science degree with a major in Electrical Engineering at Oklahoma State University in May 1995.

Experience: Employed by IBM's Federal Sector Division in Manassas, Virginia as a cooperative education student in 1990 and 1991. Worked in VLSI design department, VLSI characterization and test lab, and BSY-1 Sonar page test lab.

Currently employed by Tinker Air Force Base in Oklahoma as a civilian Electronics Engineer designing and installing secure data networks.